


# Reconstructing the Evolution of Foreland Fold-And-Thrust Belts Using U-Pb Calcite Dating: An Integrated Case-Study From the Easternmost Jura Mountains (Switzerland)

## Journal Article

**Author(s):**

Madritsch, Herfried; Looser, Nathan; Schneeberger, Raphael; Wohlwend, Stephan; [Guillong, Marcel](#) ; Malz, Alexander

**Publication date:**

2024-05

**Permanent link:**

<https://doi.org/10.3929/ethz-b-000672340>

**Rights / license:**

[Creative Commons Attribution-NonCommercial-NoDerivatives 4.0 International](#)

**Originally published in:**

Tectonics 43(5), <https://doi.org/10.1029/2023TC008181>

**Key Points:**

- Alpine deformation in the easternmost Jura Mountains is predominantly thin-skinned strongly guided by basement structures
- U-Pb calcite dating suggests thin-skinned deformation rates between 0.9 and 0.1 mm/year decreasing toward the tip of the belt
- Deformation rates appear to have decreased over time and are lower north of the main thrust front

**Supporting Information:**

Supporting Information may be found in the online version of this article.

**Correspondence to:**

H. Madritsch,  
herfried.madritsch@swisstopo.ch

**Citation:**

Madritsch, H., Looser, N., Schneeberger, R., Wohlwend, S., Guillong, M., & Malz, A. (2024). Reconstructing the evolution of foreland fold-and-thrust belts using U-Pb calcite dating: An integrated case-study from the easternmost Jura Mountains (Switzerland). *Tectonics*, 43, e2023TC008181. <https://doi.org/10.1029/2023TC008181>

Received 15 NOV 2023

Accepted 13 MAR 2024

**Author Contributions:**

**Conceptualization:** Herfried Madritsch, Nathan Looser

**Formal analysis:** Nathan Looser, Marcel Guillong, Alexander Malz

**Investigation:** Herfried Madritsch, Nathan Looser, Stephan Wohlwend, Marcel Guillong, Alexander Malz

**Resources:** Raphael Schneeberger

**Visualization:** Herfried Madritsch, Nathan Looser, Raphael Schneeberger, Stephan Wohlwend, Alexander Malz

**Writing – original draft:**

Herfried Madritsch

**Writing – review & editing:**

Nathan Looser, Raphael Schneeberger

© 2024. The Authors.

This is an open access article under the terms of the [Creative Commons Attribution-NonCommercial-NoDerivs License](#), which permits use and distribution in any medium, provided the original work is properly cited, the use is non-commercial and no modifications or adaptations are made.

This is an open access article under the terms of the [Creative Commons Attribution-NonCommercial-NoDerivs License](#), which permits use and distribution in any medium, provided the original work is properly cited, the use is non-commercial and no modifications or adaptations are made.

## Reconstructing the Evolution of Foreland Fold-And-Thrust Belts Using U-Pb Calcite Dating: An Integrated Case-Study From the Easternmost Jura Mountains (Switzerland)

Herfried Madritsch<sup>1</sup> , Nathan Looser<sup>2</sup> , Raphael Schneeberger<sup>3</sup> , Stephan Wohlwend<sup>2</sup> , Marcel Guillong<sup>2</sup> , and Alexander Malz<sup>4</sup>

<sup>1</sup>National Geological Survey of Switzerland at Swisstopo (Federal Office of Topography), Wabern, Switzerland,

<sup>2</sup>Department of Earth Sciences, ETH Zürich, Zürich, Switzerland, <sup>3</sup>Swiss National Cooperative for the Disposal of Radioactive Waste (Nagra), Wettingen, Switzerland, <sup>4</sup>Landesamt für Geologie und Bergwesen Sachsen-Anhalt, Halle (Saale), Germany

**Abstract** This case-study from the Jura Mountains in the foreland of the European Alps demonstrates how the coupling of subsurface analysis and U-Pb carbonate dating can provide absolute timing constraints and shortening rate estimates of fold-and-thrust belts. It is confirmed that the initial Late Cenozoic foreland deformation driving the formation of the easternmost Jura Mountains in Switzerland was predominately thin-skinned with contractional deformation largely restricted to the Mesozoic succession above a sub-horizontal basal décollement. Thereby, the localization and structural style of related deformation structures was strongly guided by the characteristics of underlying Late Paleozoic half grabens. The main thin-skinned thrust front formed at ~12 Ma, followed by further deformation in the hinterland and locally continued foreland-directed thrust propagation. The major deformation zones exposed at surface were established at ~8 Ma but shortening continued until at least ~4 Ma. Thick-skinned contraction associated with the inversion of basement structures only played a subordinate role during the latest deformation phase after 8 Ma. Based on cumulative shortening values derived from balanced cross sections, our U-Pb ages of syn-tectonic calcite slickenfibres allow to estimate thin-skinned deformation rates for the easternmost Jura Mountains between ~0.9 and ~0.1 mm/year, decreasing toward the eastern tip of the arcuate belt. Moreover, deformation rates seemingly decreased over time with rates of initial thin-skinned thrusting being significantly higher than the later deformation north of the main thrust front. These new findings from a classical foreland setting highlight the potential of integrating U-Pb dating in regional fold-and-thrust belt investigations elsewhere.

**Plain Language Summary** We present a case-study combining the geological-geophysical analysis of the subsurface with novel geochronological dating techniques to better constrain the evolution of the easternmost Jura Mountain in northern Switzerland. Seismic data and boreholes support the characterization of the deformation style, while dating of calcite precipitations on fractures observed in the field allow to establish deformation timing and rates.

### 1. Introduction

Deformation style, kinematics, and timing of foreland fold-and-thrust belts (FTB) are key parameters for understanding the geodynamics of convergent orogens (Nemcok et al., 2009; Poblet & Lisle, 2011). This study presents new geochronological and structural data from a classical foreland setting, the Jura FTB in the north-western foreland of the European Central Alps (Figure 1). Building on previous field work (Looser et al., 2021; Madritsch, 2015), we combine U-Pb calcite dating with the interpretation of an extensive subsurface data set (reflection seismics and drill cores) and illustrate an integrative approach to reconstruct the often polyphase tectonic evolution of FTBs. Thereby, we first focus on the analysis of the regional structural style and then use U-Pb ages of calcite slickenfibres from key field locations to constrain the formation timing and sequence of regional deformation zones. Ultimately, we establish the first absolute shortening rate estimates for the easternmost Jura FTB.

The style of contractional deformation in foreland settings is commonly ascribed to one of two end-members, termed “thin-skinned” and “thick-skinned” tectonics (Butler et al., 2018; Lacombe & Bellahsen, 2016; Pfiffner, 2006). In a thin-skinned tectonic setting, the sedimentary cover above a mechanically weak basal detachment

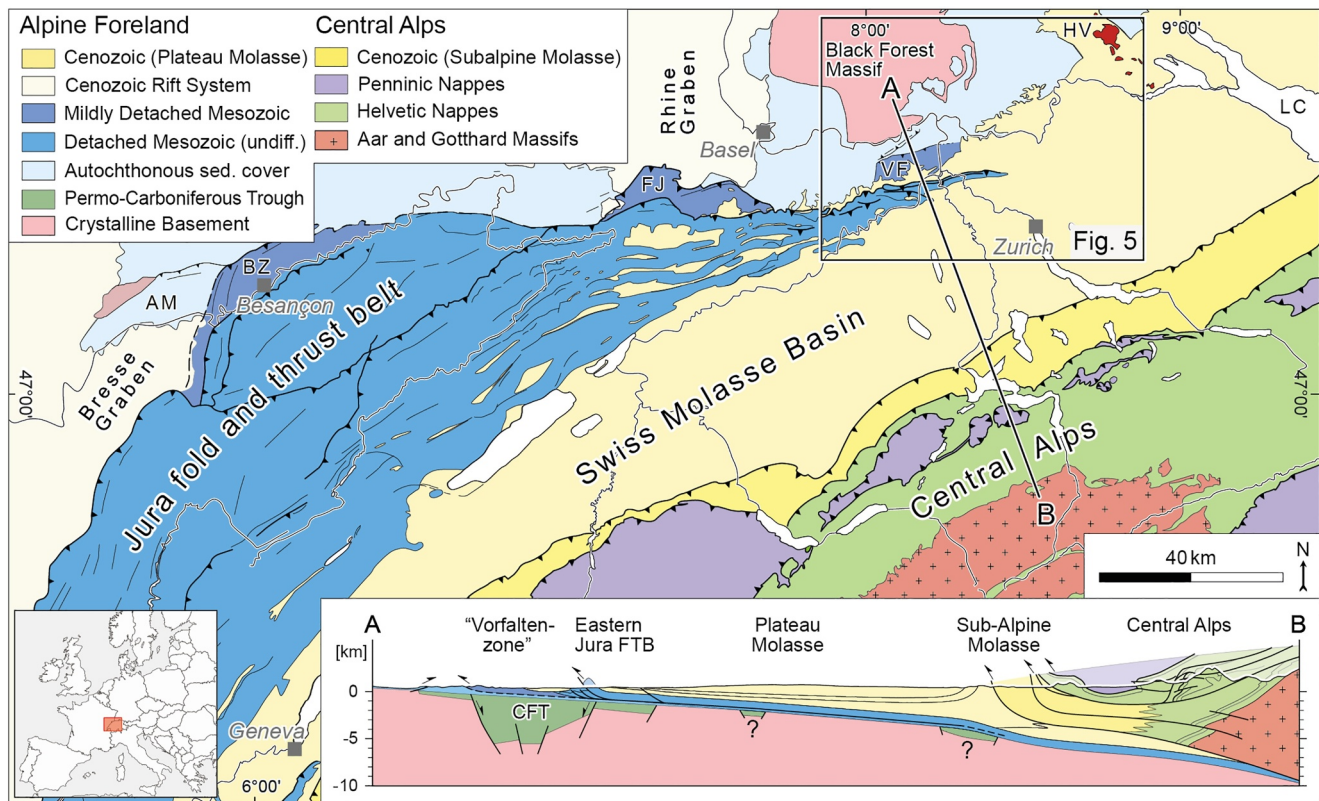


**Figure 1.** Regional setting of the study area in the northern foreland of the European Central Alps. The regional cross section marks the kinematic relationship between the thin-skinned Jura fold-and-thrust belt (FTB), and the orogenic nappe stack of the European Central Alps. Its most external parts, where the horizontal displacement along the basal décollement of the FTB is only small (<1 km) are given as mildly detached. Note that within the study area (marked by square), thrusts of the FTB often spatially coincides with deep-seated faults related the Late Paleozoic Constance-Frick Trough (CFT) hidden in the subsurface (see Figure 5 for details). AM, Avant Monts Zone (cf. Madritsch et al., 2008); BZ, Bescançon Zone (cf. Madritsch et al., 2008); FJ, Ferrette Jura (cf. Ustaszewski & Schmid, 2006); HV, Hegau Volcanics; LC, Lake Constance; VF, “Vorfalltzone” (cf. Nagra, 2014 with references therein).

horizon, referred to as “décollement” and typically constituted by evaporites or shales, is decoupled from the underlying mechanical basement composed of more competent rocks. Such thin-skinned foreland FTBs are considered to obey the laws of critical wedges (Chapple, 1978; Davis et al., 1983). On the contrary, in a thick-skinned FTB, thrusts are not decoupled but root in the underlying mechanical basement which consequently is also involved in deformation (Coward, 1983; Lacombe & Mouthereau, 2002). Despite these clear definitions, the distinction of structural styles in many foreland FTBs is often of rather hypothetic or conceptual nature (e.g., Laubscher, 1961; Pfiffner, 2017). In many cases, this is due to limited subsurface information, leaving ample room for several possible tectonic interpretations.

In both, thin-skinned and thick-skinned tectonic settings, pre-contractual foreland structures from earlier tectonic events play a key role in the evolution of FTBs. In thin-skinned settings, pre-existing faults cutting through the sedimentary sequence may offset and deform the basal décollement level and thereby hamper thrust belt propagation, trigger thrust nucleation or pre-determine the localization of transfer zones or oblique ramps during thrusting (Calamita et al., 2021; Lacombe et al., 2003; Laubscher, 1986; Malz et al., 2016; Pace et al., 2014; Tavani et al., 2021). In a thick-skinned tectonic setting, zones of pre-existing mechanical weakness within the basement can act as precursors during foreland contraction (Butler et al., 2006; Meigs et al., 2006). Indeed, for many FTBs both structural styles have been reported (Carola et al., 2015; Cristallini & Ramos, 2000; Hamilton, 1988; Lacombe et al., 2003; Madritsch et al., 2008; Molinaro et al., 2005), raising the question about their temporal relationship (see discussion in Lacombe & Bellahsen, 2016). Establishing this relationship has proven very difficult. Indications are often provided by secondary information such as geomorphological observations and/or seismological data whose temporal expressiveness is naturally limited to the most recent geological past and historical/instrumental record. Unraveling deformation timing of contractional and pre-existing non-

contractional structures in forelands represents a key aspect for assessing when and to what extent basement and cover deformation occurred and consequently, which structural style is to be invoked. The latter has important implications for the assessment of georesources and -hazards in orogenic forelands (e.g., Nemcok et al., 2009; Tavani et al., 2018).

Progress in carbonate U-Pb laser ablation inductively coupled plasma mass spectrometry (LA-ICP-MS) has opened new perspectives for the reconstruction of multiphase deformation histories in foreland settings by allowing to directly date syn-tectonic carbonate mineralizations on fault planes and provide absolute time constraints for tectonic events (e.g., Beaudoin et al., 2018; Bilau et al., 2023; Lacombe et al., 2021; Looser et al., 2021; Nuriel et al., 2017; Parrish et al., 2018; Ring & Gerdes, 2016; Smeraglia et al., 2021). Establishing a relation between carbonate veins from outcrop-scale fractures and regional structures that allow to define the tectonic characteristics of a region, such as the distinction between thin- and thick-skinned tectonics, will typically require additional constraints from field observations and/or subsurface data. When combined with tectonic strain quantifications of regional fault zones, for example, via balanced cross sections, U-Pb dating of carbonate veins can be used to estimate absolute deformation rates across FTBs (Lacombe & Beaudoin, 2023; Tavani et al., 2023).

Here, we present the results of such a combined investigation applied to the easternmost tip of the Jura FTB in Switzerland (Figure 1). This arcuate belt forms the most external part of the northwestern Alpine foreland thrust system (Schmid et al., 2004 and references therein). It is considered a classic example of a thin-skinned FTB whose formation is related to late Miocene upper crustal nappe stacking in the Central Alps (Burkhard, 1990; Burkhard & Sommaruga, 1998). According to the so-called “distant push” hypothesis (Buxtorf, 1907; Laubscher, 1961) deformation propagated into the foreland in a thin-skinned manner along a shallowly dipping thrust décollement in rheologically weak Triassic evaporites (Jordan, 1992; Sommaruga et al., 2017). While thin-skinned deformation is generally accepted as the main process behind the formation of the Jura FTB, some authors also invoked thick-skinned foreland shortening as important process in the northwestern Alpine foreland, including the reactivation and inversion of Late Paleozoic basement structures underneath the sedimentary cover of the foreland basin (Gorin et al., 1993; Madritsch et al., 2008; Mosar, 1999; Pfiffner et al., 1997; Rotstein & Schaming, 2004; Schori et al., 2021; Ustaszewski & Schmid, 2007).

For the majority of the northwestern Alpine foreland, the two deformation styles are expected to spatially overlap, often hampering a clear distinction in seismic data and leading to contradicting interpretations (cf. Giamboni et al., 2004; Mock & Herwegh, 2017; Nivière & Winter, 2000; Sommaruga et al., 2012). Precise timing constraints to temporally distinguish between the differing deformation styles are few and most often based on indirect or relative age constraints. However, several authors suggested that thick-skinned deformation only occurred during a late stage of foreland deformation (Madritsch et al., 2008; Mock & Herwegh, 2017; Mosar, 1999; Ustaszewski & Schmid, 2007). In this regard, our area of investigation is well-suited to investigate the temporal relationship between thin- and thick-skinned deformation as it encompasses the tip of the arcuate Jura FTB belt with the transition from dominantly thin-skinned foreland thrusting in the west to clearly non-decoupled basement rooted faulting further to the east (Ortner et al., 2023 with references therein). In a first step, we take advantage of a very dense subsurface data set to review the structural style of the major regional fault zones in the area and derive balanced cross sections. In a second step, we apply U-Pb dating of calcite veins from key outcrops and deep exploration boreholes to unravel their main phase of tectonic activity and to estimate foreland shortening rates. Thereby we provide a case example that illustrates how U-Pb calcite dating can be used to reconstruct the temporal evolution of foreland fold-and-thrust belts.

## 2. Regional Setting

Our area of investigation is located in northernmost Switzerland, where the eastern tip of the arcuate Jura FTB pinches out into the northern parts of the North Alpine Molasse Basin (Figure 1). This region has witnessed a polyphase tectonic history that is summarized in Figure 2 and further discussed below.

The Paleozoic basement of the region is characterized by various tectonic elements stemming from the Variscan orogeny. These deformation zones, mostly hidden in the subsurface of the northern Alpine foreland, are widely considered as important precursory structures that were reactivated during later tectonic events (Diebold & Noack, 1997; Egli et al., 2017; Laubscher, 1986; Madritsch et al., 2018; Malz et al., 2016; Mock & Herwegh, 2017; Ustaszewski & Schmid, 2007). Insights into their characteristics can be gained in the Black Forest

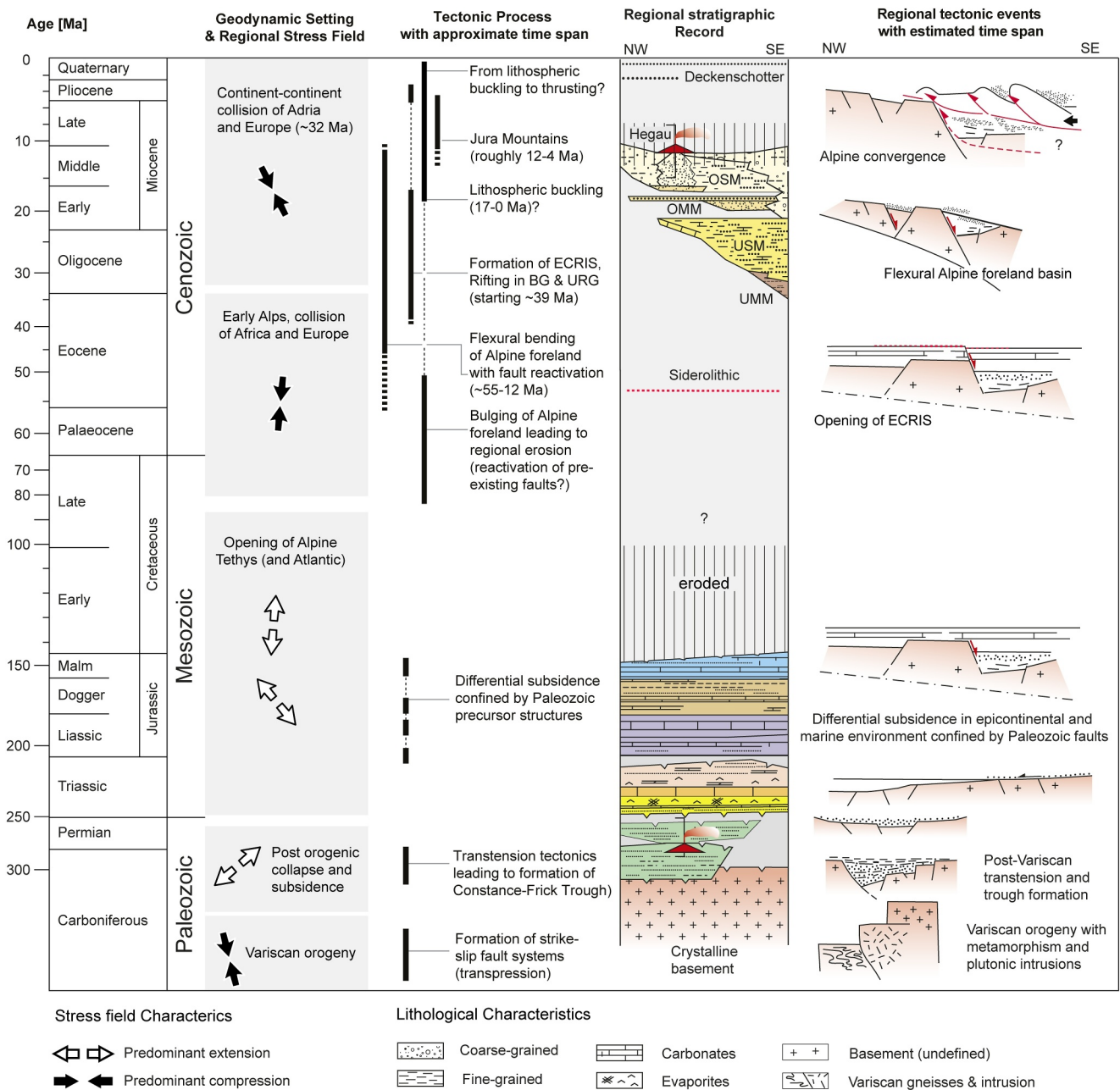


**Figure 2.** Geological evolution of the study area in context of the wider geodynamic setting. Compilation of large-scale stress field characteristics modified after Müller et al. (2002) and Schori (2022). ECRIS, European Cenozoic Rift System; BG, Bresse Graben; URG, Upper Rhine Graben.

Massif north of our study area where the crystalline basement is exposed (Figure 1). The latter is constituted by several gneiss complexes attributed to tectonic nappes stacked in S–SSW direction along regionally traceable ductile shear zones under high-temperature/low-pressure metamorphic conditions (Echtler & Chauvet, 1992; Eisbacher et al., 1989). During the latest phases of the Variscan orogeny (Figure 2), several granitic plutons intruded into the gneiss complexes and major brittle faults formed (Schaltegger, 2000; Werner & Franzke, 2001). Since Late Carboniferous times (~320 Ma), the area of investigation was rapidly exhumed (Echtler & Chauvet, 1992; Schaltegger, 2000). Post-orogenic extension resulted in the formation of Permo-Carboniferous grabens across Europe (McCann et al., 2006). In the area of investigation, one of these grabens, the Constance-Frick

Trough (CFT), stretches for tens of kilometers in a roughly ENE–WSW direction and at some places reaches depths of several-kilometers (Diebold, 1988; Madritsch et al., 2018; see cross-section in Figure 1).

After a phase of post-rifting deposition of Permian red-beds, sedimentation of the Mesozoic succession took place in an epicontinental marine environment. Periods of marine transgressions and regressions resulted in deposition of terrestrial, evaporitic, and marine sediments (see Geyer et al., 2011; Nagra, 2014 for stratigraphic overviews and related references). The Triassic sequence hosts the basal décollement of the thin-skinned Jura FTB constituted by evaporites within the Middle Triassic Muschelkalk and Upper Triassic Keuper Groups (Buxtorf, 1907; Jordan, 1992; Laubscher, 1972; Sommaruga et al., 2017). Notably, the thickness of these evaporites varies significantly due to syn-sedimentary tectonics (Marchant et al., 2005). The middle and upper Mesozoic sedimentary sequence features thick clay-rich sediments followed by increasingly calcareous rocks, including Late Jurassic massive limestones of Malm age that form the majority of exposures in the study area. Lateral thickness variations and facies changes of certain Jurassic formations have been interpreted as indication for subtle tectonic activity during their deposition (e.g., Wetzel et al., 2003). Overall, the Mesozoic sedimentary succession is marked by distinct mechanical contrasts with a strong influence on later deformation events (Malz et al., 2016; Roche et al., 2020).

The uppermost Jurassic sequence is capped by a regional unconformity spanning the Late Jurassic to Eocene sedimentary record and resulting from large-scale uplift and erosion due to the initiation of a forebulge zone associated with the Cretaceous Alpine Orogeny (Burkhard & Sommaruga, 1998; Kempf & Pfiffner, 2004; Sinclair & Allen, 1992). During Eocene and Oligocene times, the European Cenozoic Rift System evolved to the west of the study area and led to the roughly E-W directed opening of the Upper Rhine Graben (URG) (Illies, 1972; Ziegler, 1992; Figure 1). N-S to NNE-SSW striking faults occurring in high density to the west of the study area document this tectonic extension. Sedimentation resumed in Late Oligocene to Early Miocene times when the area of the Jura Mountains became part of the northern Alpine Molasse Basin (Pfiffner, 1986; Sinclair & Allen, 1992). Flexural subsidence at the distal margin of the Molasse Basin occurred simultaneously with crustal uplift in the northwards adjacent Black Forest Massif (Ziegler & Dèzes, 2006). During this process, the Late Paleozoic basement faults of the CFT, which strike roughly parallel to the Molasse Basin, were extensionally reactivated, leading to the development of normal faults and monoclines in the Mesozoic sedimentary stack (Diebold & Noack, 1997; Malz et al., 2016).

From the Middle Miocene onwards, the E-W to ESE-WNW opening of the Rhine Graben continued west of the study area (Schumacher, 2002; Ziegler & Dèzes, 2006). To the east, stratigraphic observations imply the onset of extension along NW-SE striking border faults of the Hegau-Bodensee Graben (Hofmann et al., 2000; Schreiner, 1992). It has been suggested, that this extension was assisted by an orientation change of the maximum horizontal stress axis across the northern Alpine foreland from N-S to NW-SE (Ring & Gerdes, 2016; Schori, 2022). The Hegau-Bodensee Graben also developed along pre-existing crustal-scale precursor structures traceable into the basement of the Black Forest Massif (Egli et al., 2017) and is still active today as slowly deforming zone of transtension (Diehl et al., 2022).

Thin-skinned thrusting in the external Alpine foreland related to “distant push” (Laubscher, 1961, 1972) has been inferred to have started in the late Miocene and continued into the Pliocene based on relative stratigraphic indications (~12–3 Ma; Becker, 2000 with references therein). However, recent absolute age constraints for faulting along the basal décollement from U-Pb dating of syn-tectonic calcite veins in the eastern Jura Mountains show that this process already started during Middle Miocene at 14.3 Ma the latest and lasted at least until 4.5 Ma ago (Looser et al., 2021). A similar timeframe was also reconstructed for the western Jura FTB, with calcite U-Pb ages ranging between 11.4 and 3.9 Ma (Smeraglia et al., 2021).

Thick-skinned contraction in the external Alpine foreland, as locally interpreted from seismic data, is regarded to have initiated after thin-skinned tectonics had largely ceased during Early Pliocene (Giamboni et al., 2004; Madritsch et al., 2008; Mock & Herwegh, 2017; Ustaszewski & Schmid, 2007). Thereby, timing constraints for the onset of thick-skinned deformation are mostly indirect. Nevertheless, it is well constrained by seismicity data that present-day deformation in the Alpine foreland also involves the basement (Diehl et al., 2022; Kastrop et al., 2004). Inversion of focal mechanism implies a strike-slip to normal faulting regime for the majority of the recorded seismicity. Indications for present-day compression to transpression are rare and restricted to the northwestern front of the Jura FTB, where also geomorphic expressions evidence ongoing folding (Lanza et al., 2022; Madritsch et al., 2010; Nivière & Winter, 2000).

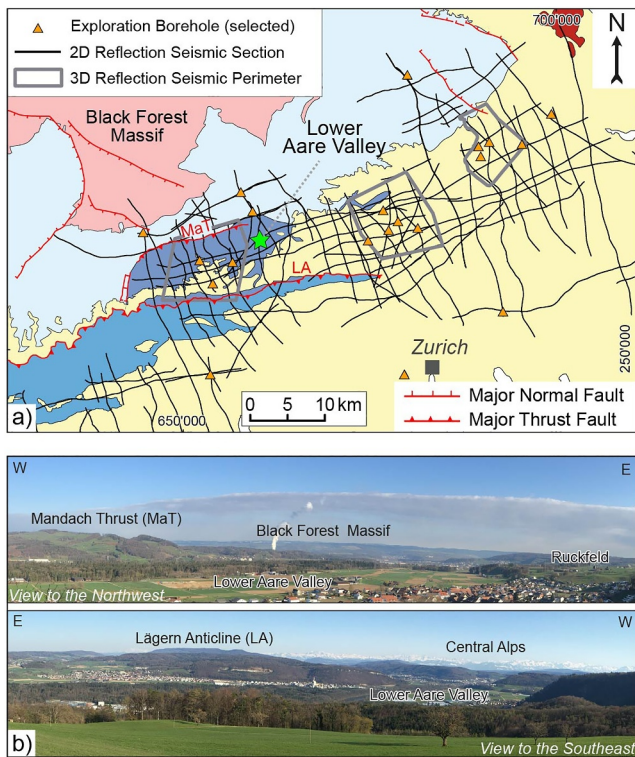


**Figure 3.** Local setting and subsurface data. (a) Data coverage map of the study area showing 2D and 3D reflection seismic data as well as selected deep exploration boreholes. The green star marks the Lower Aare Valley. See Figure 1 for full legend. (b) Panoramic views of the Lower Aare Valley in the central part of the study area (see green star in (a)) with geomorphic expressions of major regional fault zone recognizable in the field.

One reason for the difficulty to decipher the Middle Miocene to recent tectonics of the Alpine foreland is the fact that the region has been affected by regional-scale erosion since the Late Miocene (Kuhlemann & Rahn, 2013; Schlunegger & Mosar, 2011). Whether the drivers of this erosion are tectonics, climate, mantle processes or a combination thereof is under debate (Cederbom et al., 2004; von Hagke et al., 2012). In the study area, the estimated thickness of eroded sediments amounts to around 1–1.5 km (Mazurek et al., 2006), resulting in the youngest Molasse sediments preserved being approximately 9 Ma old (Rahn & Selbekk, 2007). In the area of investigation, glacio-fluvial gravel deposits of Early Quaternary age (referred to as “Deckenschotter” in Figure 2), only provide isolated indications of surface deformation beyond this time whose tectonic significance is unclear (Hammer et al., 2019). Consequently, additional absolute deformation time constraints, as can be provided by U-Pb dating of calcite slickenfibres, are of particular relevance for the reconstruction of the region’s most recent tectonic evolution.

### 3. Data and Methods

#### 3.1. Subsurface Data

The extensive subsurface data set across the study area used for its tectonic characterization is illustrated in Figure 3. It has been obtained during the exploration for a deep geological repository for nuclear waste in Switzerland carried out on behalf of the National Cooperation for Radioactive Waste Disposal in Switzerland (Nagra) since the late twentieth century. During early exploration, Nagra drilled a first series of deep boreholes and acquired 2D reflection seismic data that built up on previous prospection efforts by the oil and gas industry and drilled a first series of deep boreholes (see Nagra, 2014). Processing of the inhomogeneous seismic data set was later harmonized, including a prestack depth migration (cf. Meier et al., 2014; Nagra, 2014 with references therein). The resulting data set includes more than 80 profiles with

a total length of ~1,600 km and a line spacing of ~3 km or less. More recently, Nagra complemented its 2D seismic data set by three local 3D reflection seismic surveys (Figure 3) whose initial processing and preliminary time interpretation was previously published in Hölker and Birkhäuser (2018) and Nagra (2019a, 2019b, 2019c) respectively. For details on the related workflows, including seismic marker horizon definition and seismic-to-well tie, the reader is referred to these publicly available reports. More recently, a number of additional deep exploration boreholes penetrating the entire Cenozoic and Mesozoic stratigraphic sequence and, in some cases, also parts of the underlying Permo-Carboniferous CFT were drilled (e.g., Nagra, 2021a, 2021b, 2021c, 2022a, 2022b, 2022c, 2022d). As these new boreholes also penetrate the décollement of the Jura FTB, they provide additional insight on the regional deformation style.

#### 3.2. Sampling Strategy

Given our aim to derive age constraints for regional fault zones of distinct tectonic style, field sampling for U-Pb dating required strategy (Figure 4). It was focused on calcite slickenfibres on fracture planes indicative for syn-tectonic mineralization (Figure 4a). Despite the fact that displacement along such fractures is typically small (few millimeters), kinematic analysis allows to relate such slip increments with a tectonic setting and larger-scale deformation processes (Ferrill et al., 2021; Lacombe & Beaudoin, 2023; Tavani et al., 2015; with references therein). Ideally, slip increments on sampled slickenfibres can be directly or indirectly related to a regional deformation zone. Such relationships were successfully established in the study area and other parts of the Jura Mountains during previous paleostrain reconstructions from fault-slip pairs (Homberg et al., 1999; Madritsch et al., 2008; Radaideh & Mosar, 2021). The case-study presented here could build up on the results of a similar investigation dedicated to the detailed kinematic analysis of fracture systems observed in outcrops and interpretation of their regional tectonic context (Madritsch, 2015). The insights gained from this investigation allowed

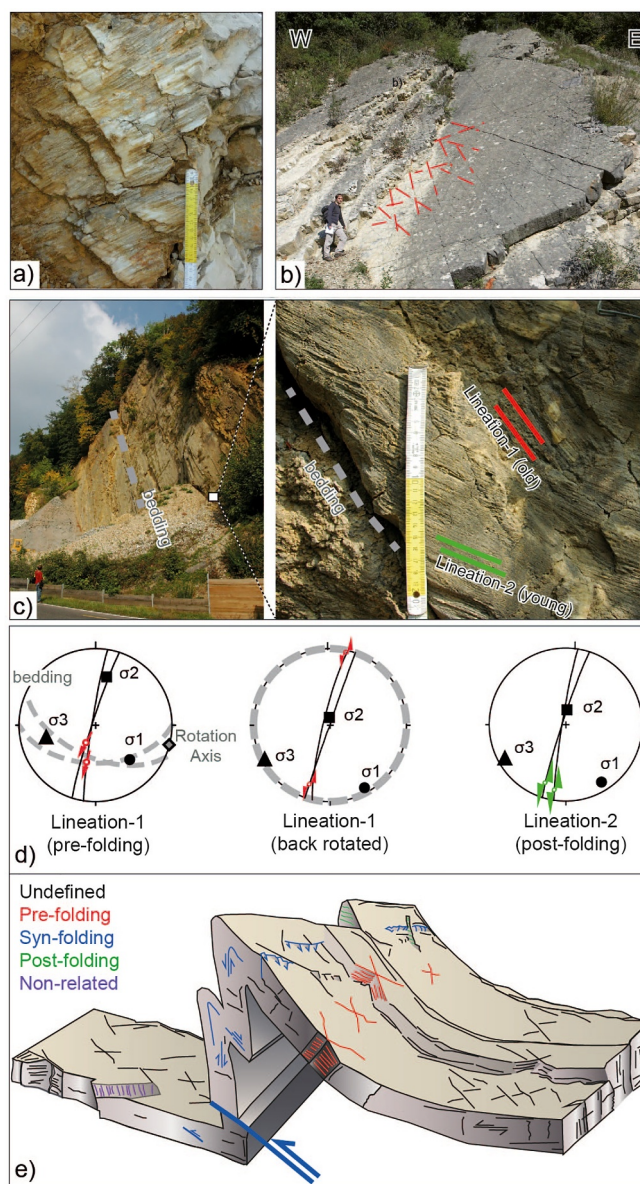


**Figure 4.** Sampling strategy for U-Pb calcite dating. (a) Calcite slickenfibres commonly found on the planes of outcrop-scale fractures within Mesozoic limestones throughout the study area. (b) Conjugated bedding-orthogonal fractures in moderately south-dipping bedding Upper Jurassic limestones (Wildeggen Formation). At this location, the latter forms the backlimb of an anticline which formed after the fractures and led to their tilting (cf. Madritsch, 2015). (c) Strike-slip fault dissecting a steeply dipping limestone succession in the eastern Jura fold-and-thrust belt (FTB). The fault plane shows two generations of slickenfibre lineations, an older one that plunges parallel to the bedding and is suspected to have formed prior to folding, and a younger, sub-horizontal one likely postdating it. (d) Fault slip analysis to validate the above interpretation. Two paleostress axes from the presumably old fault-slip pair plot on the bedding plane. After back-tilting the fault slip by the dip angle of bedding, the axes yield an orientation close to Andersonian stress state as expected in shallow crustal settings of brittle faulting. The younger fault slip pair is kinematically compatible with the same stress field, suggesting formation in a similar tectonic regime. U-Pb ages of the older slickenfibre provide a maximum age of folding, those of the younger slickenfibre a minimum age (see text for further discussion). Structural data are displayed as lower hemisphere equal area projections (modified after Madritsch, 2015). (e) Conceptual structural model outlining the relative timing relationships between various meso-scale fractures types and regional fault zones related to the Jura FTB considered during U-Pb dating sampling in the field.



us to develop a conceptual structural model outlining the relation between the various fracture types observed in outcrops and regional structures as recognized in seismic data (Figure 4).

Calcite slickenfibres of special interest are those for which relative age relationships with respect to the regional fault zones can be determined based on kinematic paleostrain analysis and geometric reconstruction of principal stress axes to an Andersonian state (Homberg et al., 1999; see Figures 4b–4d). This approach offers the potential to constrain pre-, syn- or post-slip increments with respect to strata tilting and thereby provide absolute minimum to maximum ages of related regional folding and faulting. Slickenfibres rotated with folding define a maximum age as the regional fault zones only became active after slickenfibre precipitation. Slickenfibres with slip increments postdating folded strata constrain a minimum age of the regional fault zone (Figure 4e).

### 3.3. U-Pb Calcite Dating

U-Pb dating of calcite slickenfibres was conducted by laser ablation inductively coupled plasma mass spectrometry (LA-ICP-MS) at ETH Zurich using an ASI RESOLUTION S-155, excimer (ArF, 193 nm) laser ablation system coupled to a Thermo Element XR sector-field ICP-MS, on polished chips mounted in epoxy. The analytical and data reduction procedures follow Roberts et al. (2017) using NIST SRM614 and WC-1 calcite as primary reference materials and Guillong et al. (2020) using spot sizes of 110 and 163  $\mu\text{m}$  and pulse rates of 5 and 7.4 Hz, while keeping a constant aspect ratio of the ablation craters. U-Pb dates were calculated from Tera-Wasserburg concordia lower intercepts using the IsoplotR software package (Vermeesch, 2018) and a long-term excess variance of 2% relative was propagated by quadratic addition to the uncertainty of the individual lower intercept dates (Guillong et al., 2020). ASH-15 (Nuriel et al., 2020), JT (Guillong et al., 2020), and an additional in-house secondary reference material (PDF-9B) were analyzed for validation (Table S1 in Supporting Information S1). Correction for calcite matrix effects with WC-1 was done with anchoring to 0.85 common-lead, while samples and secondary reference materials were not anchored. No disequilibrium correction was applied. All uncertainties are reported at the 95% confidence level. Prior to and after LA-ICP-MS measurements, the samples were examined by cathodoluminescence (CL) microscopy to identify growth zonings and to detect faulty ablation spots (i.e., ablation of rock matrix during analysis of thin veins) which were then excluded from the data. Lower intercept dates with a Mean Square Weighted Deviation value  $>3$  and/or an absolute uncertainty  $>10$  Ma were not considered. More details on LA-ICP-MS parameters and U-Pb metadata are reported in Table S2 in Supporting Information S1.

### 3.4. Cross-Section Balancing

Herein, we also present balanced cross-sections across the easternmost Jura Mountains so to provide geometrically viable/plausible 2D structural models that can be restored to a pre-thrusting state and provide estimates of horizontal shortening. In combination with age constraints from U-Pb calcite dating this allows to derive absolute shortening rate estimates (see discussion in Section 5.4 and Lacombe & Beaudoin, 2023 for review).

Our cross-section balancing work is grounded on the interpretation of prestack-depth migrated 2D seismic sections (Meier et al., 2014) and published geological maps of the area (Diebold et al., 2005; Graf et al., 2006). We applied classical balancing techniques of equal bed length (Dahlstrom, 1969) and constancy of areas (Mitra & Namson, 1989) to restore and geometrically validate the cross sections in an iterative manner. Given the results of our subsurface analyses (discussed in Section 5.1), we followed a thin-skinned conceptual deformation model considering the Triassic evaporites as basal décollement but also allowing for secondary detachment levels in the above-lying sedimentary cover that were found to be plausible in other parts of the Jura FTB (compare Nussbaum et al., 2017; Schori et al., 2015). For more details on our technical workflow the reader is referred to previous publications (Malz et al., 2015, 2016). The estimation of tectonic contraction along the constructed cross sections was derived by comparing the section lengths of each individual deformed section with the length of its restored section yielding to the overall shortening further discussed in Section 5.3.

## 4. Results

### 4.1. Subsurface Analyses

Based on the integrative analyses of the available subsurface data set (Section 3.1 and Figure 3), a revised tectonic map for the region was compiled (Figure 5). Of key importance for this study is the structural style of the various

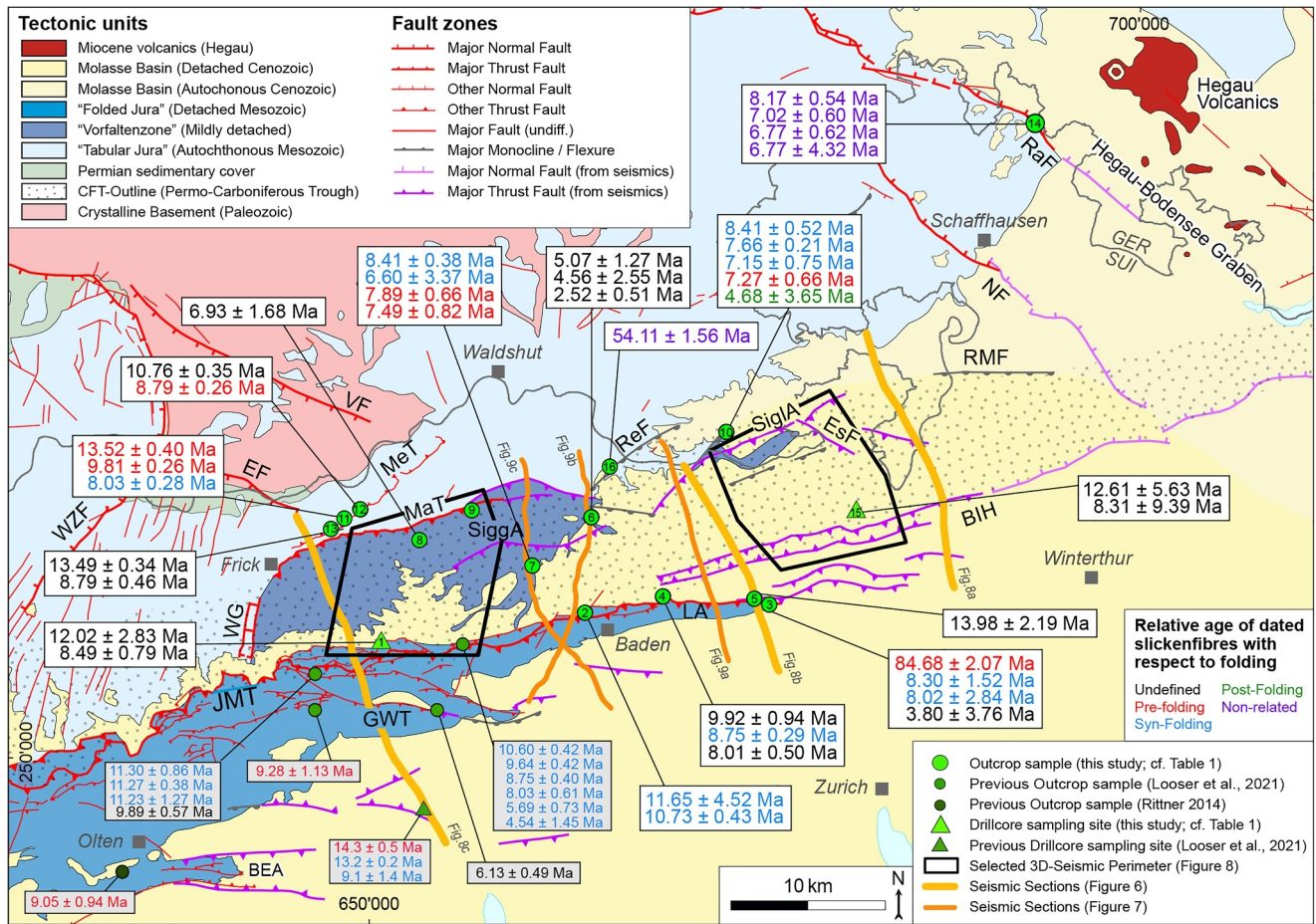


**Figure 5.** Simplified tectonic map of the study area based on the interpretation of surface and subsurface data with sample location and results of U-Pb calcite dating. The map outlines the major regional fault zones discussed in the text. Subsurface traces are sketched at the level of Top Liassic (see Figure 9 for reference). Local faults only observable within the perimeters of the local 3D seismics are not shown at this scale (cf. Figure 10). Refer to Table 1 and Supporting Information S1 for details on the sample sites for U-Pb dating from this study. U-Pb ages given in gray boxes were published previously (see legend for references). Abbreviations of regional fault zones: BIH, Baden-Irchel-Herdern Lineament; BEA, Born-Engelberg Anticline; EF, Eggberg Fault; EsF, Eglisau Fault; GWT, Gislisflue-Wildegge Thrust; JMT, Jura Main Thrust; LA, Lägern Anticline; MaT, Mandach Thrust; MeT, Mettau Thrust; NF, Neuhausen Fault; SiggA, Siggenthal Anticline; SiglA, Siglistorf Anticline; RaF, Randen Fault; Ref, Reckingen Flexure; RMF, Rafz-Marthalen Flexure; VF, Vorwald Fault; WG, Wöflinswil Graben; WZF, Wehra-Zeinigen Fault. Other abbreviations: CFT, Constance-Frick Trough.

regional deformation zones, particularly around the so-called “Vorfallenzone” just north of the main Jura FTB (“Folded Jura” in Figure 5). Given the interpretative nature of the respective seismic analyses, our results are presented as part of the discussion (Section 5.1).

#### 4.2. Field Work

According to the sampling strategy outlined in Section 3.2, 16 locations were selected for U-Pb calcite sampling. Except for the sites 9–13, all exposures are of Upper Jurassic limestones (Malm Group). In the field, we mostly sampled calcite slickenfibres from minor, outcrop-scale thrusts and strike-slip faults (Figures 6a and 6b). The displacement of these faults usually not exceeds a couple of centimeters. In addition, drill-cores from two boreholes were sampled (site 1 and 15 in Table 1 and Figure 5). The typical samples from these are mm- to a few cm-thick calcite veins (see Figure 6c for exemplary images). All details on the collected structural data are provided in Table S3 in Supporting Information S1.

Due to the unfortunate outcrop situation (see field impressions in Figure 3) it was mostly not possible to sample regional fault zones directly. One notable exception is location 14 where the regional-scale Randen Fault, a major normal fault related to the Hegau-Bodensee Graben (RaF in Figure 5), could be directly sampled (Figure 6d).

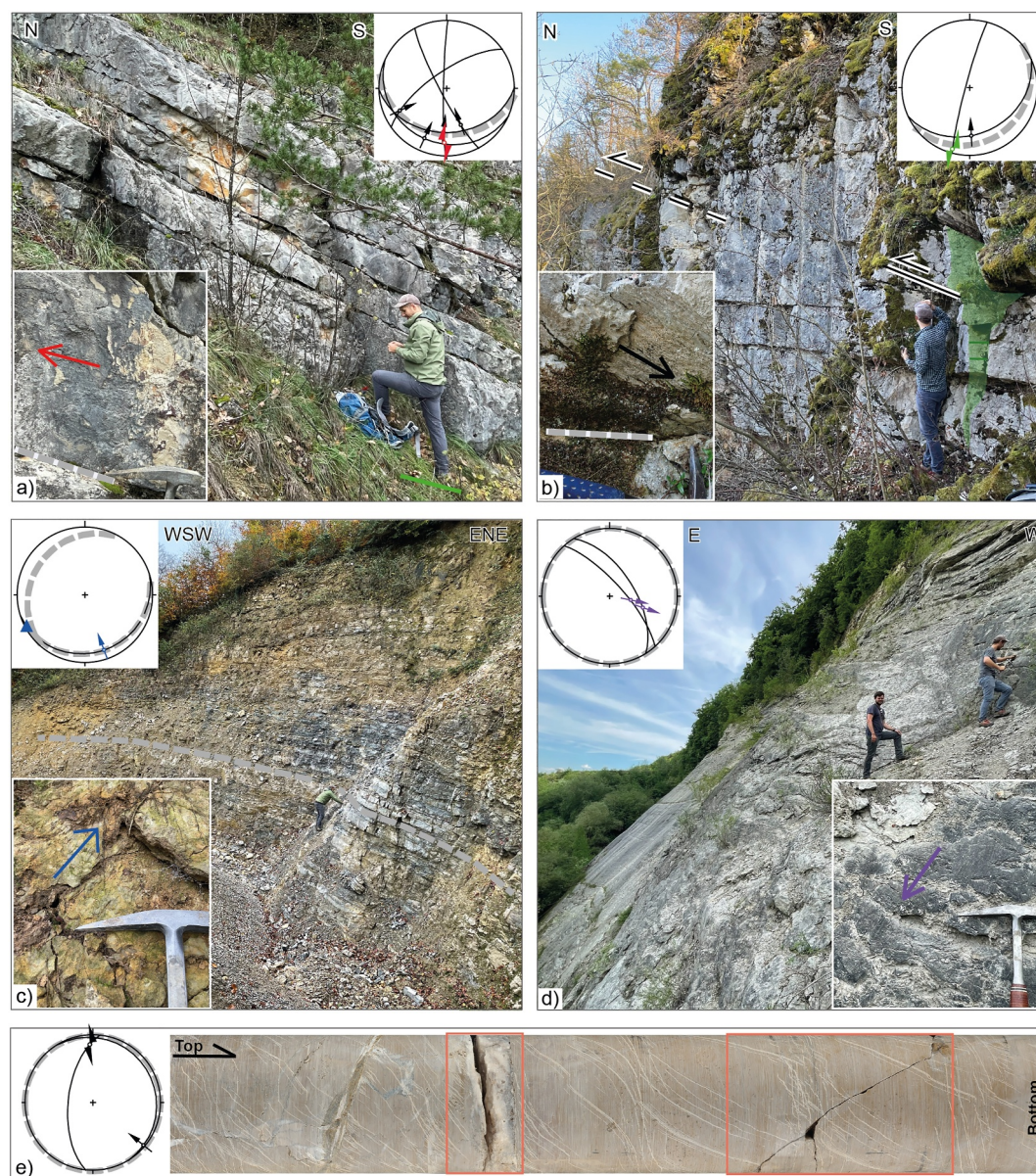


**Figure 6.** Exemplary field work results (see Figure 5 for approx. site location and Table S3 in Supporting Information S1 for more details). (a) Site 7 at the southern limb of the Siggenthal Anticline (SiggA in Figure 5): moderately south dipping Upper Jurassic limestones (Villigen Formation) featuring steep faults with slickenfibre orientations whose kinematic analyses suggests that slip occurred prior to folding (see inset with striation parallel to the bedding and compare with Figure 4). (b) Site 3 at the easternmost tip of the Lägern Anticline (LA in Figure 5): gently south dipping Upper Jurassic limestones (Burgdorf Formation) dissected by thrusts (stippled black line) and strike-slip faults (example marked in green). The relative age relationship between the thrust and folding is poorly defined, but strike-slip rather occurred after tilting of the strata indicated by the horizontal lineations unaffected by stratal tilting. Inset shows upward look at thrust fault (top to the north). (c) Site 11 located near the Mettau Thrust (MeT in Figure 5): Subtle anticline within the Upper Triassic carbonates (Schinznach Formation); anticline axis indicated by blue triangle. Inset shows bedding planes with calcite fibers interpreted as flexural slip (syn-folding). (d) Site 14 providing a large-scale exposure of the Randen Fault (RaF in Figure 5). Inset shows sampled slickenfibres indicating normal faulting (compare Table 1). (e) Drill-core of Upper Jurassic limestones (“Massenkalk”) from the exploration borehole BUL1-1 (core 556.22–557.00; Nagra, 2021a): sampled calcite bearing veins/faults (compare Table 1) are marked by squares (core diameter approx. 10 cm). All structural data are displayed as lower hemisphere equal area projections (bedding given as thick dashed line). See Figure 4 for explanation of slickenfibre color coding.

**Table 1**  
*Results of Calcite U-Pb Dating*

Deformation zone	Location & strati. position (Group)	Sample	Structure type	Rel. timing to folding	Age (Ma)	<i>n</i>
1 Jura Main Thrust	Bözberg (B2/13 borehole), Malm	BB2-98.77	Vein within tectonic slice	Undefined	12.02 ± 2.83	40
		BB2-114.65	Vein within tectonic slice	Undefined	8.49 ± 0.79	53
2 Jura Main Thrust	Bruederholz, Malm	BH-1	Bedding parallel slickenfibres in overturned fold limb	Syn-folding	10.73 ± 0.43	75
		BH-2	Bedding parallel slickenfibres in overturned fold limb	Syn-folding	11.65 ± 4.52	75
3 Lägern Anticline	Regensberg, Malm	RB-1a-Th1	Thrust fault	Undefined	3.80 ± 3.76	50
		RB-2-Th2	Thrust fault	Non-related	84.68 ± 2.07	59
		RB-3	Bedding parallel slip in outcrop-scale fold	Syn-folding	8.02 ± 2.84	68
		RB-6	Bedding-parallel thrust	Syn-folding	8.30 ± 1.52	43
4 Lägern Anticline	Oberehrendingen-Steibuck, Malm	SB-1	Thrust fault	Undefined	9.92 ± 0.94	43
		SB-2	Bedding-parallel thrust	Syn-folding	8.75 ± 0.29	53
		SB-3	Thrust fault	Undefined	8.01 ± 0.50	55
5 Lägern Anticline	Sünikon-Tüchelroos, Malm	SU-1u	Backthrust	Undefined	13.98 ± 2.19	77
6 Siggenthal Anticline	Endingen-Bad, Malm	EB-1-A	Strike-slip fault	Undefined	5.07 ± 1.27	29
		EB-1-B	Deformed strike-slip fault	Undefined	2.52 ± 0.51	25
		EB-2	Thrust fault	Undefined	4.56 ± 2.55	40
7 Siggenthal Anticline	Siggenthal-Süd, Malm	SS-3	Bedding-parallel thrust	Syn-folding	8.41 ± 0.38	75
		SS-4	Bedding-parallel thrust	Syn-folding	6.60 ± 3.37	57
		SS-5	Sin/oblique thrust fault	Pre-folding	7.89 ± 0.66	61
		SS-6	Tilted strike-slip fault	Pre-folding	7.49 ± 0.82	64
8 Mandach Thrust	Moenthal, Malm	MO-1	Strike-slip	Undefined	6.93 ± 1.68	50
9 Mandach Thrust	Mandach, Dogger	MA-1	Thrust fault	Undefined	Unsuccessful	
		MA-2	Strike-slip faults	Post-folding	Unsuccessful	
10 Siglistorf Anticline	Weilergraben, Malm	WG-1	Thrust fault	Syn-folding	7.66 ± 0.21	84
		WG-2A	Thrust fault	Syn-folding	8.41 ± 0.52	48
		WG-2B	Thrust fault	Syn-folding	7.15 ± 0.75	51
		WG-3	Strike-slip fault	Pre-folding	7.27 ± 0.66	77
		WG-4	Strike-slip fault	Post-folding	4.68 ± 3.65	48
11 Mettau Thrust	Sulzerberg-Mettau-Steinbruch, Muschelkalk	MET-1	Bedding-parallel thrust within anticline	Syn-folding	8.03 ± 0.28	45
		MET-3-young	Strike-slip fault	Pre-folding	9.81 ± 0.26	43
		MET-3-old	Strike-slip fault	Pre-folding	13.52 ± 0.40	22
12 Mettau Thrust	Sulzerberg-Mettau-Bütz, Mischelkalk	METB-1-A	Oblique thrust	Undefined	8.79 ± 0.26	50
		METB-1-B	Oblique thrust	Undefined	10.76 ± 0.35	30
13 Mettau Thrust	Sulzerberg-Zwanghau, Muschelkalk	SUB-1-B	Bedding-parallel thrust	Undefined	13.49 ± 0.34	43
		SUB-2	Strike-slip fault	Pre-folding	8.79 ± 0.46	52
14 Randen Fault	Thayngen-Lättgrueb, Malm	RA-1	Normal fault	Non-related	8.17 ± 0.54	76
		RA-2-A	Normal fault	Non-related	6.77 ± 0.62	35
		RA-2-B	Normal fault	Non-related	7.02 ± 0.60	28
		RA-3	Normal fault	Non-related	6.77 ± 4.32	37
15 BIH Lineament	Bülach (BUL1 borehole), Malm	BUL1-556.80-A	Strike-slip fault	Undefined	12.61 ± 5.63	41
		BUL1-556.80-B	Strike-slip fault	Undefined	8.31 ± 9.39	29
16 Reckingen Flexure	Reckingen-Musital, Malm	RM-2-AB	Normal fault	Non-related	54.11 ± 1.56	52

*Note.* Reported errors of U-Pb ages are  $2\sigma$ , including excess variance of 2% relative; *n* refers to the number of individual data points used for age calculation. See also Figure 5 for sample locations and Table S3 in Supporting Information S1 for more detailed information including sample site coordinates.

Elsewhere, we approached outcrops in the vicinity of the fault zones and sampled slickenfibres from minor-faults whose slip indicators were found to be compatible with the kinematics of the regional structure (e.g., compatible shortening or extension directions with respect to fold axis and fold traces; Figures 6a–6c). Dated structures of particular interest are those for which a relative chronology to the adjacent regional fault zones could be established (see further discussion in Section 5.2).

### 4.3. Absolute Age Constraints

The collected field samples were petrographically characterized, and analyzed by U-Pb LA-ICP-MS to establish absolute age constraints for the regional deformation zones. Sample locations are given in Table 1 and Table S3 in Supporting Information S1, and Figure 5. Sample photographs and CL microphotographs of all samples are presented as Supporting Information S1 (Figures S7–S14 in Supporting Information S1) together with the Tera-Wasserburg concordia diagrams of the considered and the rejected age data (Figures S1–S6 in Supporting Information S1, respectively).

#### 4.3.1. Sample Petrography

Most of the studied slickenfibres are single-phased and under CL light show homogenous colors ranging from bright to dull red and/or zoning on the same crystal (see Figures S11–S14 in Supporting Information S1). However, a few samples contain multiple phases, some of which with clear relative age constraints (cement stratigraphy, crosscutting relationships). Samples containing more than one phase and for which we obtained U-Pb ages include: EB-1 with the slickenfibre (A) being crosscut by a later fracture filled with transparent calcite of lower luminosity (B) (Figures S8g, S12d, and S12e in Supporting Information S1). WG-2 with an earlier (B) and a later (A) stage of slickenfibre growth (Figures S9f, S13a, and S13b in Supporting Information S1). MET-3 with an outer/older zone composed of small anhedral crystals (A) and an inner/younger zone with large euhedral crystals (B) (Figures S9j, S13f, and S13g in Supporting Information S1). METB-1 with a younger slickenfibre (A) crosscutting an older one (B) (Figures S9k, S13h, and S13i in Supporting Information S1). SUB-1 with a succession of an older (A) and a younger (B) calcite cement (Figures S9l, S13j, and S13k in Supporting Information S1). RA-2 with a slickenfibre (A) crosscutting an earlier vein (B) (Figures S10c, S13n, and S13o in Supporting Information S1). BUL1-556.80 with two generations of slickenfibres (A, B) with an unclear age relationship (Figures S10i, S14f, and S14g in Supporting Information S1).

#### 4.3.2. Calcite U-Pb Dating

From the 16 sampled locations (Figure 5), we obtained a total of 39 reliable ages of thrusts, strike-slip faults, and normal faults while 14 dating attempts turned out unsuccessful because of high common-lead contents or open-system behavior. The considered age data is reported in Table 1. Figure 7 shows a compilation of Tera-Wasserburg concordia diagrams for selected samples. All results, including successful as well as unsuccessful attempts are provided as Supporting Information S1 (Figures S1–S6 in Supporting Information S1).

## 5. Discussion

### 5.1. Regional Deformation Style and Influence of Basement Structures

In this section, we provide a brief structural style description for the most important regional faults zones depicted in the revised tectonic map of the study area (Figure 5) from south to north and west to east. Thereby, we focus on the characterization so-called “Vorfaltenzone,” the most external part of the Jura FTB in this area (“Folded Jura” in Figure 5; see Nagra, 2014 with references therein). The discussion is supported by a series of depth-migrated seismic sections (Figures 8 and 9) and selected horizon time slices of local 3D seismics (Figure 10). Moreover, selected drill core images from the stratigraphic horizons widely considered to constitute the basal décollement of the Jura FTB belt are presented in Figure 11. A synoptic illustration of the relationship between regional faults zone observed within the Mesozoic sedimentary cover and the underlying basement structures is presented in Figure 12, supported by balanced geological cross sections (Figure 13).

The eastern tip of the Jura FTB (“Folded Jura” in Figures 5 and 12) is a narrow zone of deformation marked by closely spaced and mostly ENE-striking thrust stacks and tight thrust-related folds that are well-traceable in the field (Diebold et al., 2005; Graf et al., 2006). The main frontal deformation zone is referred to as “Jura Main

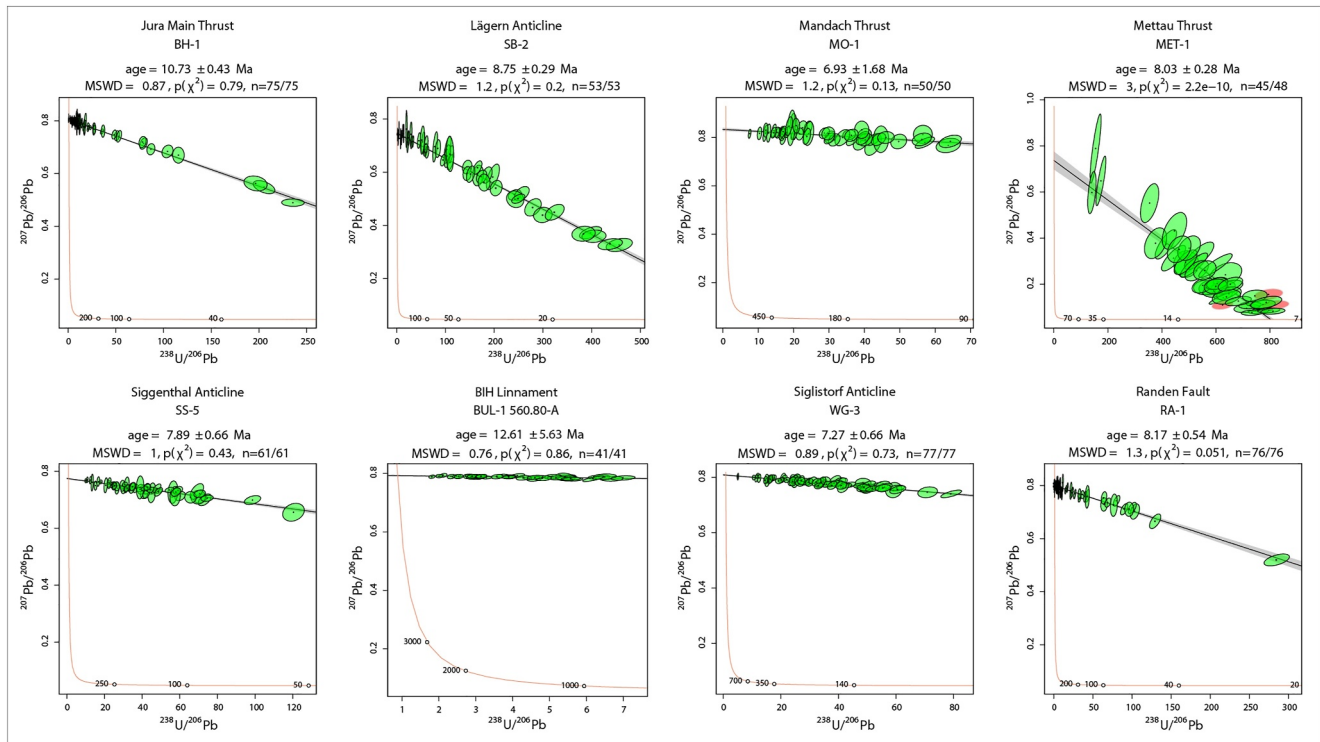


**Figure 7.** Tera-Wasserburg concordia diagrams for selected field samples. Compare with Table 1 for sample details, Figure 5 for location and Supporting Information S1 for more sample details. Reported uncertainties are 95% confidence intervals including 2% long-term excess variance (Guillong et al., 2020).

Thrust” (JMT in Figures 5 and 12) along which the basal décollement of the FTB is exposed. Its eastward continuation is represented by the so-called Lägern Anticline (LA in Figures 3, 5, and 12). Although the seismic data across these structures does not allow to robustly determine much structural details (Malz et al., 2015, 2016), a thin-skinned deformation style, as promoted by pioneering investigators (Buxtorf, 1907; Laubscher, 1986), was found to be admissible for the eastern Jura FTB on the basis of 2D cross section balancing (Jordan et al., 2015 and references therein). There is no clear evidence for an active involvement of the basement underneath these structures during Miocene shortening. Nevertheless, the localization of the thrust-belt front has long been thought to be controlled by pre-thrusting normal faults inherited from the southern boundary of the Permo-Carboniferous CFT (Diebold et al., 1991; Laubscher, 1986; Malz et al., 2016; Naef et al., 1995; indicated in Figure 12). While in the western part of the study area, there are no clear indications for such pre-existing normal faults, and the Mesozoic strata north and south of the main thrust belt shows no major vertical offset (Figure 8c; Malz et al., 2015), this is indeed the case in the more central part (Figure 9).

The western part of the so-called “Vorfallenzzone” north of the Jura Main Thrust, is bounded by the Mandach Thrust (MaT in Figures 5 and 12) some 6 km further north. It strikes roughly E-W and can be traced at the surface for ~15 km (Diebold et al., 2005; Graf et al., 2006). Previous investigations showed that the Mandach Thrust is located above a major normal fault zone rooting in the basement (Bitterli-Brunner, 1987; Laubscher, 1986). Malz et al. (2019) carried out a detailed analysis of the Mandach Thrust using cross section balancing on the basis of a dense grid of depth-migrated 2D seismic sections and confirmed that it was strongly influenced by this pre-existing normal fault but can nevertheless be interpreted as a thrust branching from a basal décollement in Triassic strata (Figures 8c, 9b, and 9c). Newly available data to verify the interpretation of such shallow-rooted thrusting north of the Jura Main Thrust comes from 3D seismic data and drill cores from the presumed basal décollement of Jura FTB (Figures 10 and 11). The former revealed a folded Top Muschelkalk horizon just above the Middle Triassic evaporites of the Zeglingen Formation (Figure 10). In addition, drill cores from the borehole BOZ-1-1 show pervasive viscous deformation across the short halite section within this formation (strongly recrystallized halite), but also in the thicker anhydritic section of the overlying Bänkerjoch Formation (stretched anhydrite and boudinaged clay layers, Figures 11d–11h). Both findings strongly support the interpretation of a

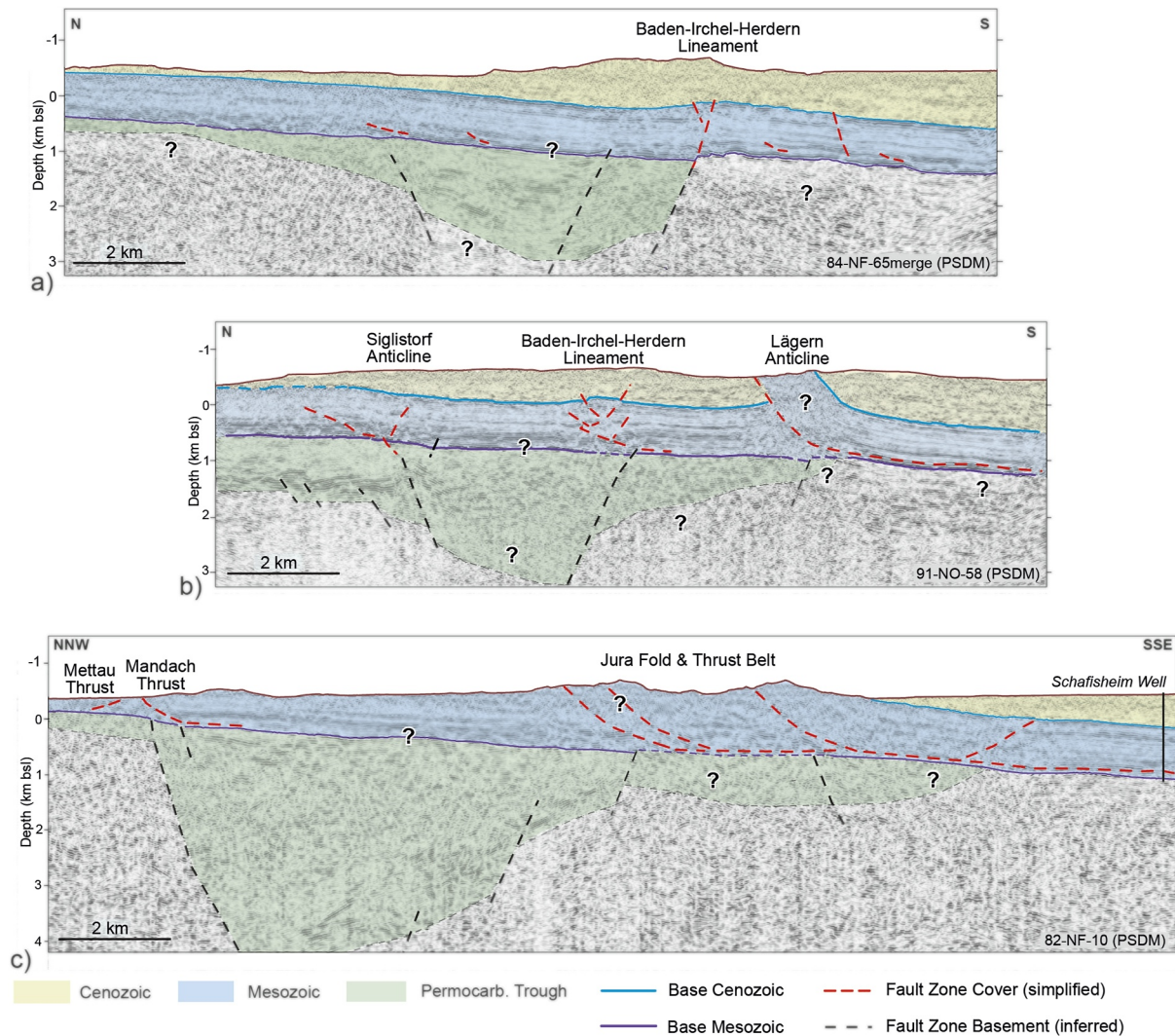


**Figure 8.** Regional seismic section across the study area with very simplified interpretation to illustrate the principal deformation style across the study area (modified after Meier et al., 2014). The shown seismic sections are prestack depth-migrated (PSDM) and presented from east to west (see Figure 5 for location). Section designation according to Meier et al. (2014): (a) Seismic Section 84-NF-65 where almost no seismic-scale expression of Alpine foreland shortening related to the Jura fold-and-thrust belt (FTB) is recognizable; (b) Seismic Section 91-NO-58 crossing the Lägern Anticline in eastern part of the “Vorfallenzone”; (c) Seismic Section 82-NF-10 crossing the Schafisheim well where the basal décollement of the Jura FTB was encountered (Jordan, 1992) and dated (Looser et al., 2021) and the western “Vorfallenzone.”

thin-skinned deformation style in this region. Consequently, the area between the Jura Main Thrust and the Mandach Thrust must be considered to be mildly detached (~200–400 m of shortening along the basal décollement; Malz et al., 2019). We suggest that thin-skinned thrust propagation occurred in a similar manner as described for the Ferrette Jura where N-S striking normal faults related to the URG are interpreted to have acted as transfer faults during Miocene thin-skinned thrusting (Figure 1; Ustaszewski & Schmid, 2006). The Wölflinswil Graben (WG in Figure 12) is a likely candidate for a kinematically similar transfer fault. Smaller-scale faults of similar orientation are also recognizable on the Top Muschelkalk horizon slices of the western 3D seismic data set (left image in Figure 10).

The SE verging “Mettau Thrust” (MeT in Figures 5 and 12), located ~2 km north of the Mandach Thrust, is a peculiar contractional structure due to its isolated location and NE-SW strike and was interpreted controversially in the past. Some authors interpreted this structure as toe of a gravitational nappe that slid off the Black Forest rift shoulder (Bitterli-Brunner, 1987; Wildi, 1975; see Diebold et al., 2005 for a discussion) whereas others proposed that it formed in the context of contractional Alpine foreland tectonics (e.g., thin-skinned back-thrust, Jordan

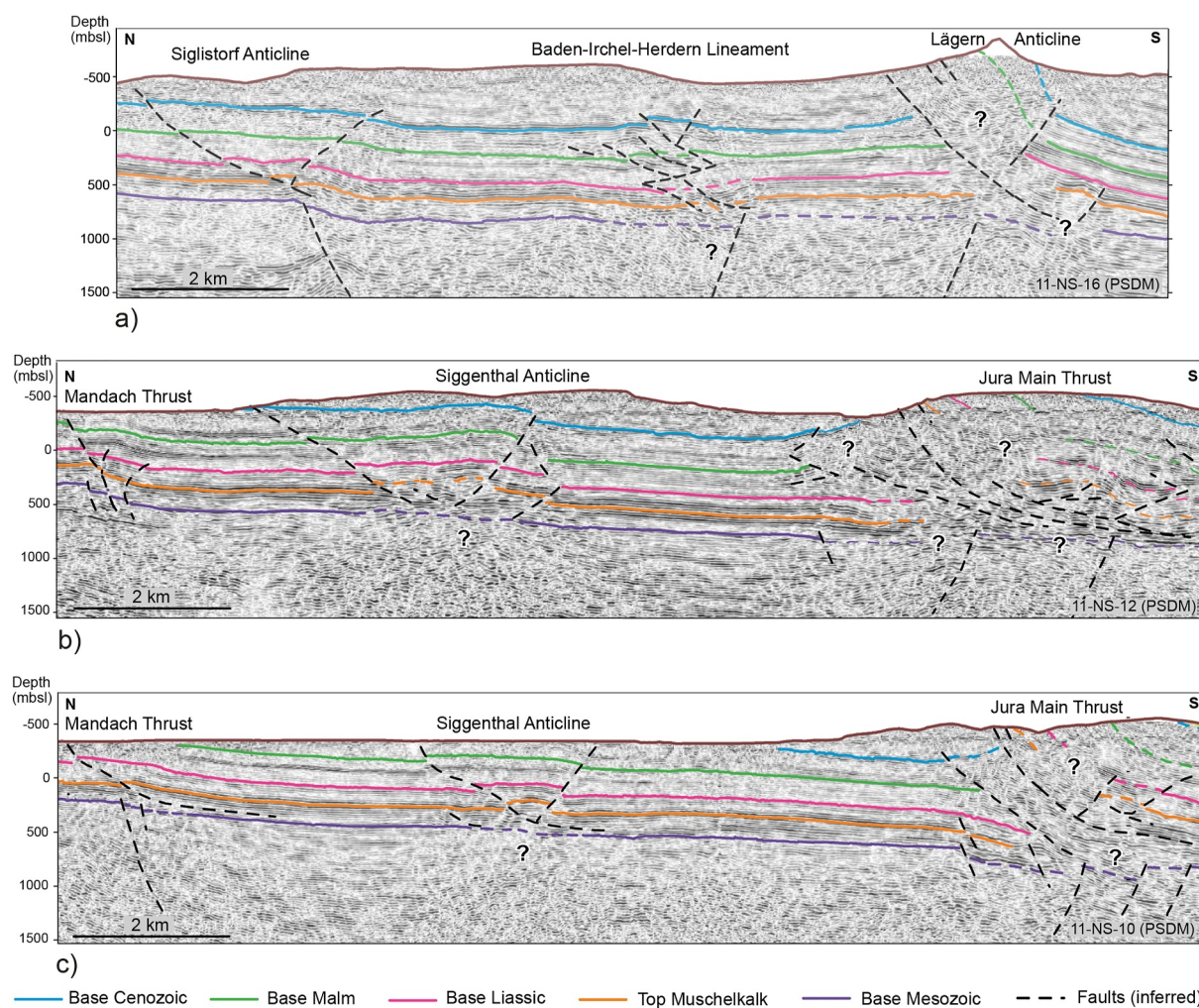


**Figure 9.** Local seismic sections from the central part of the “Vorfalltzone” with seismic interpretation (modified after Meier et al., 2014). The shown seismic sections (all prestack depth-migrated; PSDM) are located in the central part of the study area (see Figure 5 for location in between the seismic sections shown in Figures 8b and 8c) and presented from east to west. Section designation according to Meier et al. (2014): (a) Seismic Section 11-NS-16; (b) Seismic Section 11-NS-12; (c) Seismic Section 11-NS-10. A laterally variable deformation style of selected regional fault zones can be observed (see text for discussion).

et al., 2015 and references therein). The available seismic data does not allow for an unambiguous structural characterization of this structure (Figure 8c). We will therefore base its further interpretation on our new U-Pb calcite ages (see Section 5.3).

The N-S striking lower Aare Valley (Figure 3), cuts orthogonally through the thrusts of the Jura FTB and has long been thought to mark the location of a tear fault, as similarly reported for the more westerly parts of the range (Laubscher, 1961; Radaideh & Mosar, 2021; Schori, 2022). To some extent, this hypothesis was inspired by the apparently abrupt termination of the Mandach Thrust west of the valley (Bitterli-Brunner, 1987). More recent E-W striking 2D seismic sections crossing the valley did not provide evidence for a major N-S striking fault system (Nagra, 2014 and reference therein). Instead, it was observed that the Mandach Thrust continues across the valley with the thrust-displacement gradually decreasing further to the east until only the normal fault precursor structure is observable (see Figure 9). Moreover, the structure bends toward SE at the intersection with a major Paleozoic fault zone exposed in the northward-adjacent Black Forest Massif (the so-called Vorwald Fault; VF in Figure 5; cf. Madritsch et al., 2018). Further to the south, the “Siggenthal Anticline” (SiggA in Figures 5 and 12) is exposed at the surface (cf. Figure 3). In contrast to the Mandach Thrust, seismic data indicates that this structure dies out toward the west but continues eastward (Figures 9 and 10). It cannot be linked to a major basement structure and is therefore considered a décollement-based structure within the “Vorfalltzone.” Overall, shortening along the Mandach



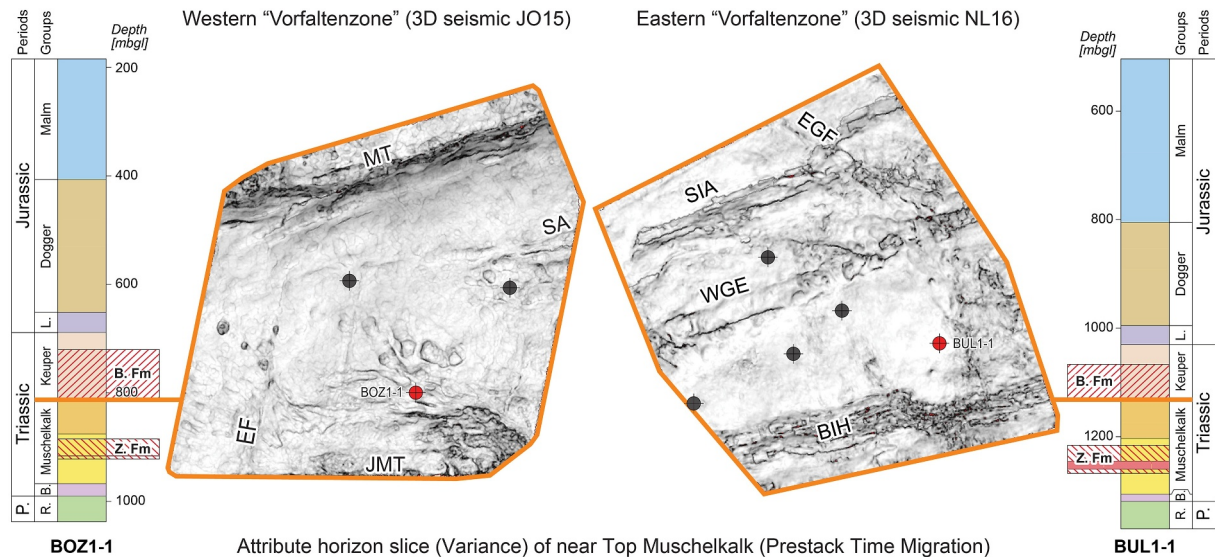


**Figure 10.** 3D seismic images from the western and eastern “Vorfallenzone” with annotated expressions of regional deformation zones and selected Nagra exploration boreholes (modified after Nagra (2019a, 2019b)). Polar dip attribute horizon time slices of the near-Top Muschelkalk (stratigraphic location indicated in the borehole section) for the Nagra 3D seismic data sets JO15 and NL16 (see Figures 3 and 5 for location of the seismic perimeters) with selected seismic-scale faults indicated by black lines (see Nagra, 2019a, 2019b for full interpretation details). Schematic profiles of selected Nagra boreholes, only drilled after the seismic interpretation shown here, highlight the stratigraphic units that host the evaporitic detachment horizons of the Jura fold-and-thrust belt (FTB) including the Zeglingen and Bänkerjoch Formation (compare Figure 11). Abbreviations: EF, Effingen Fault; MaT, Mandach Thurst; SiggA, Siggenthal Anticline; JMT, Jura Main Thrust; SigIA, Siglistorf Anticline; WGE, Weiach-Glattfelden-Eglisau Fault; EsF, Eglisau Fault; BIH, Baden-Irchel-Herdern Lineament; P, Permian; R, Rotliegendes; B, Buntsandstein Group; L, Lias Group; B. Fm, Bänkerjoch Formation; Z. Fm, Zeglingen Formation.

Thrust decreases across the lower Aare Valley from west to east while the Siggenthal Anticline gradually increases in structural elevation and width (Figure 9). This structural configuration is interpreted as indication for a soft linkage between the Mandach Thrust and the Siggenthal Anticline, as often observed in thin-skinned FTBs (Dahlstrom, 1969; Watkins et al., 2017). The array of structures implies a local back-stepping of thin-skinned deformation within the “Vorfallenzone” from west to east. This is to be expected when envisaging thrust propagation transfer along N-S striking normal faults in the west (see discussion in Ustaszewski and Schmid (2006) for comparison). The eastward continuation of the Siggenthal Anticline remains unclear due to one of the few remaining larger gaps in seismic data coverage (Figure 3). Considering the similar structural style (Figures 9a and 9b), a connection with the more easterly Siglistorf Anticline appears likely (see further discussion below).

In the eastern part of the “Vorfallenzone,” Cenozoic deposits cover the Mesozoic succession Nevertheless, the main fault zones are clearly expressed and consistently imaged by 2D and 3D seismic data (Nagra, 2014, 2019b; Figures 8–10). Immediately north of the Lägern Anticline, the “Baden-Irchel-Herdern Lineament” (BIH in Figures 5 and 12), can be traced with an E-W strike for tens of kilometers. Malz et al. (2016) suggested that it represents a partly inverted normal fault that itself inherited from a Late Paleozoic precursor structure, namely the southern bounding fault of the CFT (Figures 8b, 9a, and 12). The same authors interpreted that the contractional overprinting of the normal fault by thin-skinned tectonics coupled with the strong mechanical layering of the Mesozoic sequence (Roche et al., 2020) led to the formation of a complex triangle zone (Figure 9). Since the BIH is completely buried underneath Molasse deposits no sample material for U-Pb calcite dating is available. Samples of veins considered representative for the latest contractional deformation phase of this structure were obtained from the nearby Nagra exploration borehole BUL1 (Figure 10). This borehole penetrated a several meter-thick karstified zone close to the top of the Mesozoic sequence with clear evidence for tectonic deformation (dark blue line in the borehole section of BUL-1-1 in Figure 10; Gegg et al., 2020; Nagra, 2019b, 2021a). The calcite veins sampled some 10 m below this deformation zone (Figure 6e) are further discussed in Section 5.2.

The northern boundary of the eastern part of the “Vorfallenzone” is again located above the northern bounding fault of the Permo-Carboniferous CFT Constance-Frick Trough (Figure 8c). However, in contrast to the west

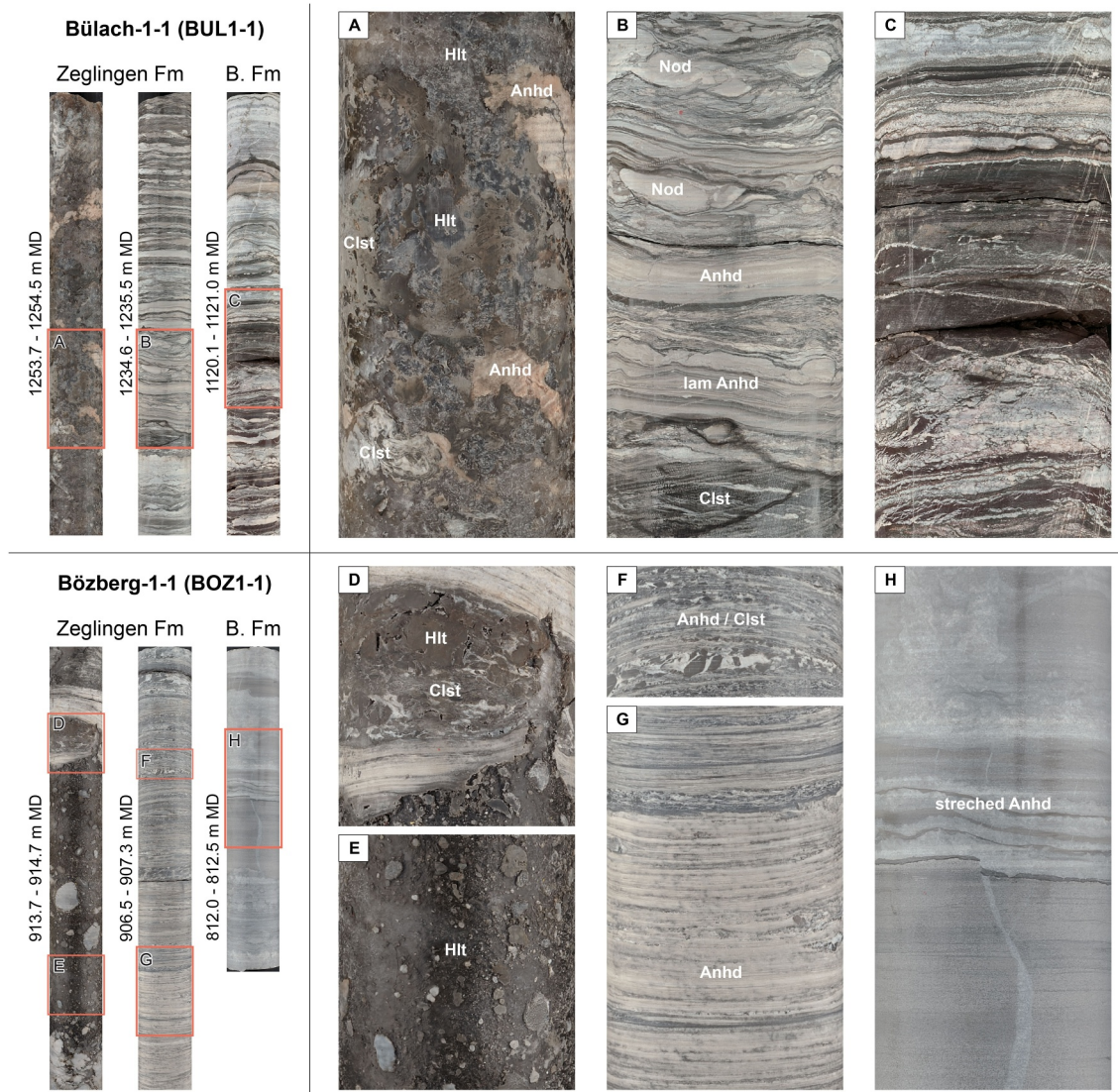


**Figure 11.** Selected drill cores of the Middle to Upper Triassic evaporites from the Nagra exploration boreholes BUL1-1 (a–c) and BOZ1-1 (d–h). All cores have a diameter of 95 mm (modified from Nagra (2021a, 2022a)). (a) Foliated halite with angular claystone clasts partially showing winged inclusions in recrystallized halite, (b) Sedimentary structures in the Middle Triassic Zeglingen Formation indicating the absence of penetrative viscous deformation, (c) Dolomitic to argillaceous marl of the Bänkerjoch Fm. With multiple mirror-like fault planes indicative for shearing, (d) Halite-clay breccia in the Zeglingen Fm, (e) Halite section shows fine grained recrystallized matrix with larger rounded clay clasts, (f) Anhydrite-clay intercalation with foliated anhydrite and stretched clay layers (dark gray) forming boudins, (g) Anhydrite section in the Middle Triassic Zeglingen Formation showing foliated anhydrite with stretched clay indicative of penetrative viscous deformation, (h) Upper Triassic Bänkerjoch Formation with stretched anhydrite layers above a normal fault indicating low strain viscous deformation. Abbreviations: MD, Measured depth; Hlt, Halite; Clst, Claystone; Nod, Nodule; Anhd, Anhydrite; lam Anhd, Laminated anhydrite; B. Fm., Bänkerjoch Formation.

where it is marked by the narrow Mandach Thrust, a substantially broader deformation zone is developed here, characterized by a monocline of the Mesozoic strata (Figures 5 and 12). 3D seismic data revealed two distinct fault zones cutting through the latter (Nagra, 2019b and Figure 10; right image). The previously recognized, regionally traceable “Siglistorf Anticline” in the north (SiglA in Figures 5, 8b, 9a, and 10; Naef et al., 1995), is a gentle antiform characterized by shallow NW- to N vergent thrusts in its core affecting the Triassic and Jurassic strata (Figure 9a). The second fault zone further south, which was only recently identified based on the 3D seismic data, is the “Weiach-Glattfelden-Eglisau Lineament” (WGE in Figure 10; Nagra, 2019b). This ENE-WSW striking and sub-vertical fault zone, only observed within the 3D-seismic perimeter (compare adjacent 2D seismic section in Figure 9a), is reported to cut through the basal décollement of the Jura FTB and be linked to basement faults related to the Late Paleozoic CFT (Schöpfer et al., 2023). Thereby, the WGE locally separates the

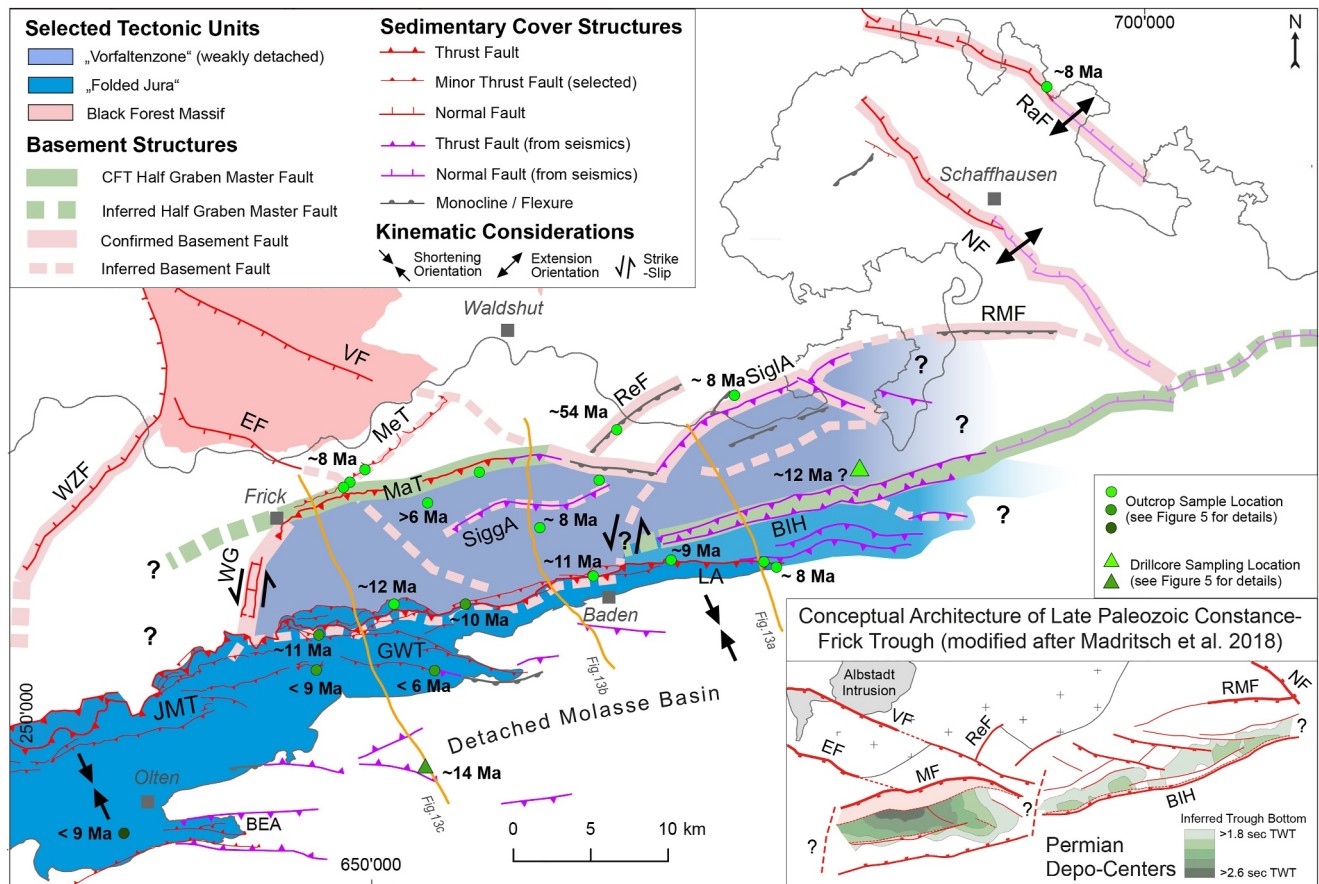


**Figure 12.** Synoptic tectonic map illustrating the spatial and kinematic relationship between regional fault zones in the sedimentary cover and basement and approximate age constraints provided by U-Pb calcite dating. Deformation age estimates for regional fault zones given here are simplified aiming to illustrate a tectonic model (Figures 14 and 15; for details refer to Figure 5 and Table 1). Inset shows Permian depocenters as indicated by regional seismic interpretation in time domain (TWT, two-way-travel time); refer to Figure 8 for local depth estimates. See text for further discussion. Fault zone abbreviations: BEA, Born-Engelberg Anticline; EF, Eggberg Fault; GWT, Gislisflue-Wildegg Thrust; JMT, Jura Main Thrust; LA, Lägern Anticline; MaT, Mandach Thrust; MF, Mandach Fault (CFT border fault); MeT, Mettau Thrust; NF, Neuhausen Fault; RaF, Randen Fault; ReF, Reckingen Flexure; RMF, Rafz-Marthalen Flexur; SiggA, Siggenthal Anticline; SigLA, Siglistorf Anticline; VF, Vorwald Fault; WG, Wölflinswil Graben; WZF, Wehra-Zeinigen Fault.

Siglistorf Anticline from the other presumably thin-skinned structures further to the south (e.g., the BIH; Figure 10). Due to this observation, Schöpfer et al. (2023) suggested that the Siglistorf Anticline may represent a basement-rooted contraction structure as well. However, more recent drilling results of Nagra provided good indications that at least some shear deformation along the basal décollement has propagated beyond the BIH. Small amounts of viscous deformation are observed in single layers within the comparatively thick halite sections as well as in shear fracturing within clay layers of the Bänkerjoch Formation (Figures 11a and 11c). Also from a regional tectonic perspective, similarities in structural style strongly suggest that the Siglistorf Anticline indeed represents the eastward continuation of the shallow-rooted Siggenthal Anticline (Figures 9a and 9c). Kinematically, such an interpretation implies that basement rooted deformation locally observed along the clearly basement-rooted WGE only occurred during a relatively late-stage deformation phase, post-dating the earlier propagation of thrusting along the Triassic décollement (compare discussion in Schöpfer et al., 2023).

The lateral variation of structural style across the “Vorfallenzzone” discussed above is interpreted to be guided by pre-existing structures in the Mesozoic succession that themselves are related to the structural configuration of the Permo-Carboniferous CFT (Figure 1). The polarity of this basement graben changes from east to west (Figures 8 and 12; Madritsch et al., 2018). In relation to this polarity change, the localization of its post-Paleozoic reactivation varies as well. In the west, no substantial basement fault reactivation is evident underneath the Jura Main Thrust (Figures 8c and 13c; Malz et al., 2015). Thin-skinned deformation has clearly propagated beyond the southern graben boundary into the “Vorfallenzzone” (Figures 10 and 11). A distinctly

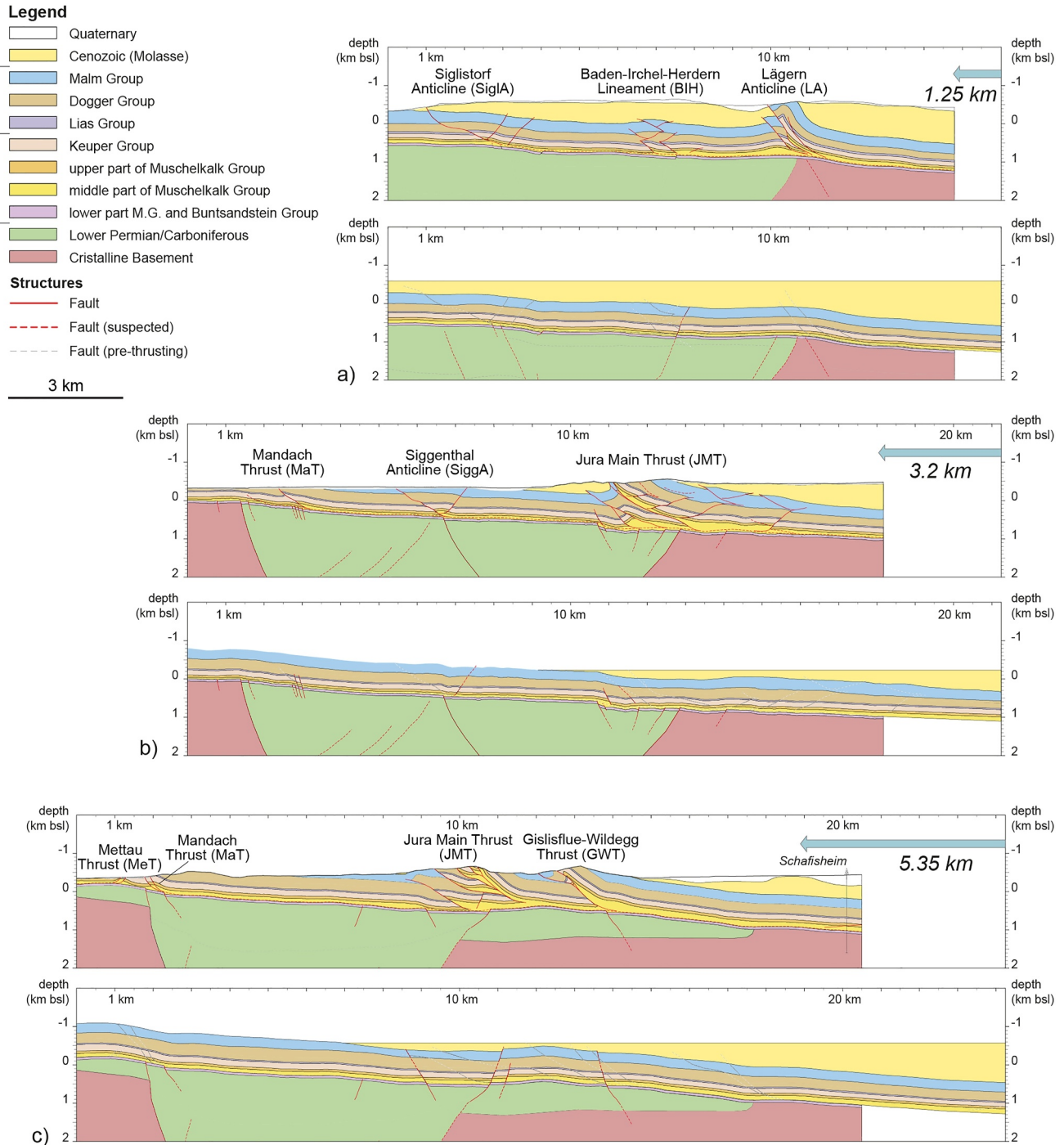


**Figure 13.** Balanced and restored regional cross section through the study area (see Figure 12 for location). (a) Eastern cross section along seismic profile 91-NO-58 (cf. Figure 8b); (b) middle section along seismic profile 11-NS-10 (Figure 9c) and (c) western cross section along seismic profile 82-NF30 (cf. Figure 8c). The top images show the deformed section constructed under consideration of field and subsurface data (primarily seismic interpretations by Meier et al. (2014)) and applying constant line-length area balancing techniques; bottom images show the same section restored to a pre-thrusting state (see Malz et al. (2015) for methodological outline).

reactivated normal fault is only observed north where the main CFT half graben fault is found underneath the Mandach Thrust. In the eastern “Vorfallenzzone,” where the CFT half graben has an opposite polarity, a clearly reactivated normal fault is located at the southern rim of the graben underneath the BIH lineament (Figure 8b). According to borehole information, the area north of the BIH was only affected by minor décollement-related

thrusting associated with horizontal Anticline appear to die out gradually. The same accounts for the compressional overprint of the BIH while the precursor normal fault can be traced for several kilometers further (Figure 5; Malz et al., 2016). Whether this is also the case for the WGE and the Siglistorf Anticline further north remains unclear. A series of NW-SE trending faults including the Eglisau Fault (EsF in Figures 5, 10, and 12; Nagra, 2019b) apparently lead to a stronger degree of segmentation in this area. In any case, the “Rafz-Marthalen Flexure” even further to the east (RMF in Figure 5) is a monocline also associated with the northern boundary of the CFT showing no more clear seismic indication for a contractional overprint (cf. Naef et al., 1995; Nagra, 2019c). It is cross-cut by NW-SE striking Neuhausen Fault (NF in Figure 5) representing the easternmost border fault of the Hegau-Bodensee Graben (Egli et al., 2017). While this fault is not well exposed at surface, the more easterly Randen Fault (RaF in Figure 5) crops out east of Schaffhausen (site 14 in Figure 5; see also Figure 6d). This allowed direct fault sampling for U-Pb dating and to assess the temporal relationship between demonstrable basement-rooted normal faulting in this area and the previously described contractional structures of the “Vorfaltenzone” (see further discussion below).

## 5.2. Absolute Timing Constraints for Regional Deformation Zones From U-Pb Calcite Dating

The deformation ages from calcite slickenfibres obtained during this study and previously published by Looser et al. (2021) provide key time constraints on the activity range of the investigated regional fault zones. In the following, the obtained slickenfibre ages (Figure 5, Table 1, and Supporting Information S1) are interpreted with the aim to derive formation age estimates for the regional deformation zones (see Section 3.1 and Figure 4 for the principal interpretation concept).

The first absolute age constraints for deformation along the basal décollement of the Jura FTB provided by Looser et al. (2021) were from the Schafisheim borehole located ~5 km south of the Jura Main Thrust in the Molasse Basin and from outcrops in the Jura FTB (Figures 5 and 8c). Accordingly, thin-skinned deformation initiated at 14.3 Ma at the latest and lasted at least until 4.5 Ma. For thrusting along the Jura Main Thrust, these authors constrain an activity span of at least ~7 Ma (11.3–4.5 Ma). Our new U-Pb ages for the Jura Main Thrust of  $12.02 \pm 2.83$  and  $8.49 \pm 0.79$  Ma from the B2/13 borehole (site 1 in Figure 5 and Table 1), which penetrates a splay of the Jura Main Thrust, and of  $11.65 \pm 4.52$  and  $10.73 \pm 0.43$  Ma from an exposure of folded strata at the location Bruederholz (cf. site 2 in Figure 5 and Table 1 and Table S3 in Supporting Information S1) both fit well into the previously established activity range.

Constraining the age of the Mandach Thrust turned out to be challenging as only iron-oolites of the Upper Dogger (Ifenthal Formation; Diebold et al., 2005) with slickenfibres of low U and high common Pb contents are exposed along its hanging wall. Three attempts (site 5 in Figure 5; MA-1a, MA-1b, MA-2; Figures S5g, S5h, and S5i in Supporting Information S1) did not provide reliable age data. A slickenfibre from the back limb of the thrust-related fold at Mönthal (site 8 in Figure 5; MO-1; Table 1, Figure 5) yielded an age of  $6.93 \pm 1.68$  Ma but the relation of this slip increment with thrust formation remains undefined given the very gentle regional dip at this location.

The Mettau Thrust was sampled at several exposures of the Triassic Schinznach Formation located along the fault trace (Figure 6c). A bedding parallel slickenfibre from an exposed anticline in the hanging wall of the thrust with an age of  $8.03 \pm 0.28$  (site 11 and MET-1; Table 1; see Figure 6d) is interpreted as good estimate for the formation age of the structure. Another slickenfibre from the same outcrop but with clear pre-folding relationship (MET-3; Table 1) yielding ages of  $13.52 \pm 0.40$  Ma and  $9.81 \pm 0.26$  Ma is in agreement with this interpretation.

East of the lower Aare Valley, the Siggenthal Anticline was sampled in an outcrop of its southern limb (Figures 3 and 6a; site 7 in Figure 5 and Table 1). Four samples were dated successfully yielding ages ranging from  $8.41 \pm 0.38$  to  $6.6 \pm 3.37$ . As these slickenfibres are either bedding parallel thrusts or affected by the folding of the strata they are clearly syn- to pre-folding. Two more successfully dated slickenfibres were collected in exposures along the northern limb of the Siggenthal Anticline (site 6 in Figure 5 and Table 1) where a subtle tilting of Upper Mesozoic limestones associated with small-scale thrust faults is observed (Madritsch, 2015). While being significantly younger with ages of  $5.07 \pm 1.27$  and  $4.56 \pm 2.55$  Ma (EB-1-A and EB-1B in Table 1) they are still in good agreement with the activity time span of thin-skinned thrusting previously provided by Looser et al. (2021). At  $2.52 \pm 0.51$  Ma, one of the dated slickenfibres experienced additional deformation as is recorded by a small crack with a later generation of vein calcite perpendicular to the fault plane (see Figures S8g, S12d, and S12e in Supporting Information S1). However, a kinematic relation to foreland shortening of this late deformation event is

not clear. On the other side of the age spectrum, a normal fault sampled in a nearby outcrop of the Recking Flexure (ReF in Figures 5 and 11) yielded an age of  $54.11 \pm 1.56$  Ma (site 16; RM-2-AB; Table 1). This is very well in line with a formation of this extensional deformation zone in the context of the pre-thrusting tectonic history of the region (cf. Section 2 and Figure 2).

Further to the east, additional samples from the main deformation front of the eastern Jura FTB were collected along the Lägern Anticline (Figures 3 and 5). Three dated slickenfibres at location Oberehrendingen-Steibuck (site 4 in Figure 5 and Table 1), where the overturned limb of the anticline is exposed, are related to flexural slip during the formation of the anticline. The U-Pb ages allowed us to constrain a formation of the anticline between  $9.92 \pm 0.94$  and  $8.01 \pm 0.50$  Ma (SB-1, SB-2, SB-3-AB; Table 1) and are in good agreement with the results of Looser et al. (2021). At the locations Sünikon-Tüchelroos and Regensberg (sites 5 and 3 in Figure 5 respectively), five more ages between  $13.98 \pm 2.19$  (SU1u-AB) and  $3.80 \pm 3.76$  (RB-1a-Th1) were obtained. Among them, the age of  $8.02 \pm 2.84$  Ma for sample RB-3 stems from a bedding-parallel slickenfibre within an outcrop-scale local fold and is regarded the most representative age for the formation of the Lägern Anticline (~8 Ma). Younger thrust faulting recorded in the same outcrop (RB-1a-Th1) is being interpreted as an expression of further fold tightening. Another result worth discussing from the Regensberg location is the unexpectedly old age of  $84.68 \pm 2.07$  Ma for sample RB-2-Th2. This age was obtained from a sparry vein cement bounding the actual slickenfibre on the fault plane (Figure S7i in Supporting Information S1). However, differences in luminosity under CL light between the slickenfibre and the sparry vein cement (Figure S11i in Supporting Information S1) as well as the fact that the sparry cement, in contrast to the slickenfibre, yielded high U and low common Pb contents indicate that these phases are distinct and formed during different points in time. We thus interpret the  $84.68 \pm 2.07$  Ma to represent an older vein fill whose kinematic context remains unknown. The compressively overprinted BIH north of the Lägern Anticline was not accessible for direct sampling. The veins and slickenfibres sampled in the nearby borehole BUL1-1 are taken into account as indication here given their proximity to a tectonically deformed zone (Gegg et al., 2020; Nagra, 2021a; Figure 6e) previously interpreted as splay thrust of the BIH (Nagra, 2019b). Unfortunately, most of our dating attempts of small-scale structures around this deformation zone remained unsuccessful (see Supporting Information S1). Two samples taken from small-scale strike-slip faults approximately 15 m underneath the main deformation zone (see Figure 6e) yielded ages of  $12.61 \pm 5.63$  and  $8.31 \pm 9.39$  Ma (cf. Table 1). The low precision of the two ages from the vicinity of the BIH do not allow for a robust age estimate for this deformation zone. Nevertheless, a comparatively old age for the BIH would be in agreement with the kinematic interpretation of Malz et al. (2016) that this peculiar triangle zone above the southern boundary of the Late Paleozoic CFT formed relatively early (12 Ma?), prior to the southward-adjacent Lägern Anticline.

The formation age of the Siglistorf Anticline further north is well constrained by samples from the location Weilergraben (site 10 in Figure 5; see Table 1 and Table S3 in Supporting Information S1). Syn-folding slickenfibres suggest formation of the anticline around 8 Ma (between  $8.41 \pm 0.52$  and  $7.15 \pm 0.75$  Ma; WG-1AB, WG-2A, WG-2B; Table 1). A post-folding strike-slip related slickenfibre of  $4.68 \pm 3.65$  from the same location Ma (WG-4; Table 1) is well in agreement with this interpretation.

Finally, four U-Pb ages of slickenfibres sampled directly from the fault plane of the Randen Fault in the easternmost part of study area (site 14 in Figure 5) constrain that the main activity of this basement rooted normal fault occurred between  $8.17 \pm 0.54$  and  $6.77 \pm 0.62$  Ma (RA-1 -2 and -3; cf. Table 1). The young ages are well in line with still ongoing activity of the Hegau-Bodensee Graben suggested by seismological data (Diehl et al., 2022).

### 5.3. Integrative Interpretation of Deformation History and Sequence

Our data set allows to reconstruct the Middle—Late Miocene deformation history at the eastern tip of the Jura Mountains in an unprecedented level of detail. Figure 14 shows a series of sketch maps outlining the evolution of the study area in time. Figure 15 shows conceptual sketches of our interpretation for the western, central, and eastern part of the “Vorfallenzzone.” Both figures focus on the deformation of the Mesozoic cover in relation to the underlying basement. The Cenozoic overburden is deliberately excluded given the uncertainties regarding the timing of its late-stage erosion (Mazurek et al., 2006; von Hagke et al., 2012).

Prior to Alpine foreland deformation (e.g., >14 Ma; top map in Figure 14), the study area was already dissected by normal faults related to earlier tectonic events (cf. Section 2 and Figure 2). According to Looser et al. (2021) who dated deformation along the basal décollement at the location of Schafisheim (Figures 8c, 12, and 14), thrusting

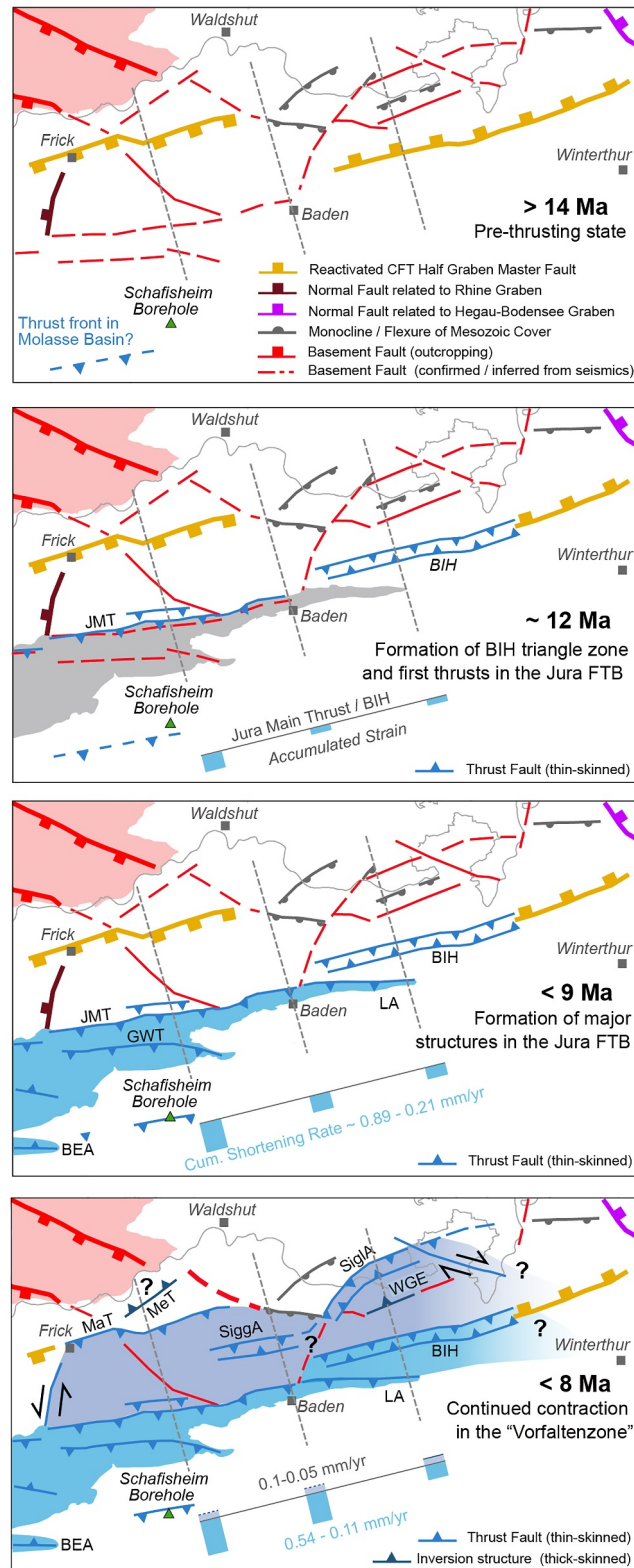


**Figure 14.** Sketch maps of the study area illustrating its temporal evolution according to the results of this study. Accumulated strain north and south of the Jura Main Thrust and Baden-Irchel-Herdern Lineament (BIH) not to scale. Stippled lines indicate approximate location of sketch sections shown in Figure 15. See Figure 12 for explanation of fault zone abbreviations and text for further discussion, particular the derivation of cumulative (cum.) shortening rates.

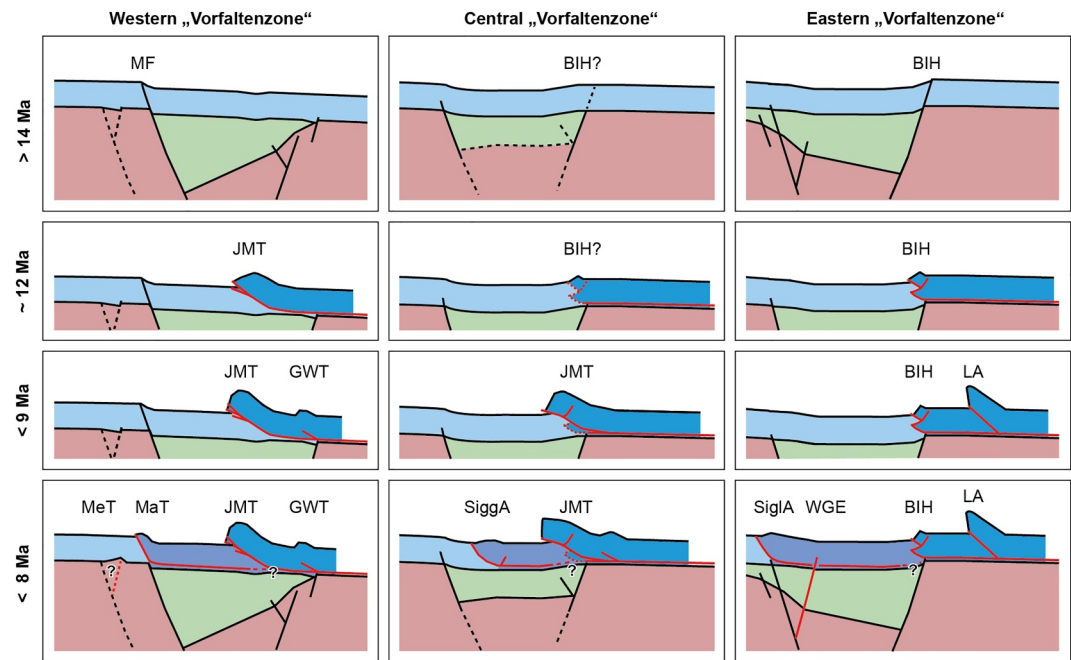


**Figure 15.** Conceptual sketches illustrating the deformation sequence across the “Vorfalltazone” and the adjacent Jura fold-and-thrust belt in the easternmost Jura Mountains (Cenozoic Molasse overburden not shown). See Figure 14 for approximate location, Figure 12 for explanation of fault zone abbreviations and text for further discussion.

within the Molasse basin onset at  $\sim 14.3$  Ma the latest. The main activity of the Jura Main Thrust further north seems to have started 3–5 Ma later (Figure 14). Looser et al. (2021) reported thrust increments at the Jura Main Thrust as old as  $11.3 \pm 0.9$  Ma but showed that the main phase of deformation and folding occurred after  $9.3 \pm 1.1$  Ma based on rotated strike-slip faults. It is worth noting that our new data from the Jura Main Thrust with ages of up to  $12.0 \pm 2.8$  Ma at the B2/13 borehole also indicate that the most frontal thrusts along the main front of the Jura FTB formed relatively early, followed by the formation of thrusts in the hinterland in an out-of-sequence manner (Figures 14 and 15). This is in good agreement with the maximum age of 9.8 Ma for the even further south located Born-Engelberg Anticline (Figure 5; Madritsch, 2015; Rittner, 2013) and previous interpretations of the Jura FTB evolution (e.g., Sommaruga, 1999).

Slickenfibres dated in the vicinity of the Lägern Anticline do not provide a robust maximum age estimate for the structure itself but show that meso-scale thrusting occurred between  $9.92 \pm 0.94$  Ma to  $8.02 \pm 2.84$  Ma with the structure presumably being formed around the same time ( $\sim 9$ –8 Ma). Taking into account the previous age estimate of around 12 Ma for the northward adjacent BIH based on kinematic considerations (Malz et al., 2016) also implies out-of-sequence thin-skinned deformation in this part of the “Vorfalltazone” (Figures 14 and 15).

Folding north of the Jura Main Thrust and the BIH occurred after  $\sim 12$  Ma. For example, folded slickenfibres along the Siggenthal Anticline (e.g., site 7, sample SS6  $7.49 \pm 0.82$  Ma; cf. Table 1) indicate that here, folding occurred only after  $\sim 8$  Ma. The youngest deformation ages with clear kinematic relation to foreland shortening around the northern limb of the Siggenthal Anticline of  $5.07 \pm 1.27$  and  $4.56 \pm 2.55$  Ma (site 6; compare Table 1 and Figure 5) are in very good agreement with the activity range for the décollement at the Jura Main Thrust provided by Looser et al. (2021) lasting until at least 4.5 Ma.

In the first place, the above-described deformation occurred along regional deformation zones marked by shallow-rooted, listric thrusts. At some point however, basement rooted faults became active as well in response to stresses exerted by the Alpine collision as witnessed by the formation of the WGE (Schöpfer et al., 2023). As outlined earlier, we infer that this happened only after the formation of the Siglistorf Anticline (e.g., later than 8 Ma; Figures 12, 14, and 15). At the same time there is also evidence for normal slip along the Randen Fault (although there are stratigraphic indications that this structure has already formed in Early Miocene times as indicated in



Figure 14; Hofmann et al., 2000). The apparent simultaneity of extensional to transtensional faulting along the Randen Fault and contraction within the neighboring “Vorfaltenzone” implies that the region witnessed distinct strain partitioning across the investigated area at that time (Egli et al., 2017). The associated Late Miocene stress field was marked by a rather stable orientation of the maximum horizontal stress axis (roughly trending NNW-SSE; see Figure 12; cf. Madritsch, 2015). Hence, strain partitioning was likely enabled by a switch in the orientation of the minimum horizontal stress axis from vertical in the west to a horizontal ENE-WSW trend in the east. The Mettau Thrust deserves special emphasis because of its controversial interpretation in the past (Bitterli-Brunner, 1987; Laubscher, 1986; Wildi, 1975). According to our U-Pb calcite data it formed at approx.  $8.03 \pm 0.28$  (see discussion in Section 5.2). This formation age is well compatible with the activity of shallow rooted thrusting in the western part of the “Vorfaltenzone” (Mandach Thrust, Siggenthal Anticline). We therefore conclude that this structure is not a gravitational slide in relation to the Early Miocene uplift Black Forest Uplift as interpreted by some earlier investigators but instead related to Alpine foreland tectonics. The style of contractional deformation along it remains unclear due to the absence of expressive seismic data. However, given its orientation oblique to the thin-skinned thrust front formed by the Mandach Thrust but parallel to a number of basement-rooted extensional flexures further to the east and west (WFZ and ReF in Figures 5 and 12), a strong control of pre-existing basement structures, possibly involving their late-stage reactivation can be inferred (Figures 14 and 15).

Overall, our new age data implies that the intensively deformed thin-skinned belt (“Folded Jura” in Figure 12) and the more external “Vorfaltenzone” were deformed sequentially (Figures 14 and 15) but also, that deformation in general oscillated across the belt. That being stated, horizontal bedding parallel slip increments within the upper part of the Muschelkalk Group (Schinznach Formation) north of the Mandach Thrust are as old as 13.5 Ma (samples MET-3-old and SUB-1B; Table 1). This may suggest that Alpine deformation along the basal décollement propagated far into the foreland at an early point in time, before the regional structures evolved (therefore not indicated in Figure 14). On the other hand, the minor amount of shortening observed within the “Vorfaltenzone” question whether this deformation has really been transferred all the way from the distant Alps (e.g., according to initial hypothesis by Buxtorf, 1907) or is rather rooted more proximal underneath the Jura FTB (Figure 15) or within the Molasse Basin (Mock & Herwegh, 2017; Pfiffner et al., 1997).

#### 5.4. Estimation of Shortening Rates

The regional shortening derived from balanced cross sections (Figure 13) together with the newly available absolute deformation ages of regional deformation zones allows us to estimate shortening rates for this part of the Jura FTB.

In the western part of the study area, shortening across the main Jura FTB and the “Vorfaltenzone” accumulates to  $\sim 5,350$  m (Figure 13c). Considering the main deformation phase occurring between  $\sim 14.3$  Ma (recorded at Schafisheim; Looser et al., 2021) and  $\sim 8$  Ma (the presumed end of pure thin-skinned tectonics), yields a maximum cumulative thin-skinned shortening rate of  $\sim 0.89$  mm/year. However, as reported by Looser et al. (2021), shortening continued until at least  $4.5 \pm 1.5$  Ma, in agreement with the youngest thrust-slickenfibres from the “Vorfaltenzone” dated in this study at  $4.56 \pm 2.55$  Ma (site 6; Table 1 and Figure 5). Considering this longer period of time (roughly  $\sim 14$  to  $\sim 4$  Ma), results in a cumulative deformation rate of  $\sim 0.54$  mm/year.

Estimates of shortening across the eastern part of the study area (Figure 13a) must again built on the onset of deformation  $\sim 14.3$  Ma ago as recorded at Schafisheim. Cumulative shortening across this section is comparatively well constrained at  $\sim 1,250$  m. Termination of thin-skinned thrusting at around  $\sim 8$  Ma, respectively  $\sim 4$  Ma, results in rate estimates of 0.21 and 0.11 mm/year.

Notably, these different shortening rates are largely driven by the substantial decrease of shortening along the Jura Main Thrust from west to east (from  $\sim 5,000$  to  $\sim 800$  m; Figure 13) which is in good agreement with the regional trend observed across the western Alpine foreland (Burkhard, 1990; Laubscher, 1961). For the northward adjacent “Vorfaltenzone,” however, shortening values are roughly constant between 200 and 400 m (cf. Malz et al., 2016, 2019). Taking our deformation sequence into account suggesting that this shortening occurred only between  $\sim 8$  and  $\sim 4$  Ma (Figures 14 and 15), leads to a constant but much lower shortening rate of 0.10 to 0.05 mm/year.

It appears, that shortening rates were comparatively high at the beginning of foreland thrusting. Thereby they gradually decreased toward the tip of the arcuate Jura FTB. In the study area, the shortening occurring after

formation of the more intensively deformed “Folded Jura” (Figure 12) in the more external “Vorfallzone” was characterized by much slower rates.

### 5.5. Correlation and Interpretation in the Alpine Context

Our new deformation sequence of the easternmost Jura Mountains based on U-Pb calcite dating fits very well in the Alpine orogenic context of the Jura FTB. As discussed by Looser et al. (2021), the early onset of deformation along the basal décollement of the Jura FTB already at 14.3 Ma is corroborated by field observations of early-stage foreland shortening close to the Alpine front (Beck et al., 1998; Deville et al., 1994). The evidence of thrusting along the décollement at 13.2 Ma at the latest (Looser et al., 2021) is in good agreement with major shortening pulses in the Sub Alpine Molasse (starting at 12 Ma and more pronounced at 10–5 Ma, Mock et al., 2020; von Hagke et al., 2012) and horizontal shortening the Central Alps (12–13 Ma, Herwegh et al., 2019). The main phase of thin-skinned deformation (i.e., large-scale folding and thrusting) occurring after 9 Ma as shown in this study further confirms the findings of Looser et al. (2021) and Smeraglia et al. (2021) obtained by direct U-Pb dating and previous indirect timing estimates (Becker, 2000; Malz et al., 2016 with references therein).

Our data shows that thick-skinned deformation in the Alpine foreland initiated some time after ~8 Ma, possibly earlier than previously inferred from geomorphic indications (~4 Ma, Giamboni et al., 2004; Madritsch et al., 2008; Ustaszewski & Schmid, 2007). By that time, deep-seated deformation in the Alpine foreland was active contemporaneously with ongoing shortening in the sedimentary sequence along the basal décollement. This could be explained by changes in foreland wedge mechanics, hypothetically exerted by the breaking of the thin-skinned thrust front or large-scale erosion processes (Mosar, 1999). However, as demonstrated here, the Jura Main Thrust in our study area was active significantly earlier (at ~11 Ma at the latest) and recent thermochronological ( $\Delta_{47}/(U-Pb)$ ) data by Looser et al. (2021) implies that any large-scale erosion occurred later, not before 4.5 Ma. Therefore, we consider that the observed thick-skinned deformation, comparatively minor after all, could alternatively be driven by even deeper crustal processes. The slap breakoff model for the Alpine orogen (Herwegh et al., 2019; Kissling & Schlunegger, 2018) invokes a strong impact on the stress field in the external foreland potentially driving fault reactivation. Because of the coevality of basement rooted faulting along the CFT and extension in the Hegau-Bodensee Graben, we consider this scenario more likely. Thereby, the kinematics of pre-existing faults in the foreland appear to be controlled by their orientation with respect to far-field stresses exerted onto the shallow foreland crust by mantle dynamics underneath the orogen in the hinterland.

## 6. Conclusions

The results of our study allowed for a detailed reconstruction of the Miocene deformation history at the eastern tip of the Jura Mountains in the northwestern foreland of the European Alps. The extensive subsurface data set across this area allowed for a detailed structural characterization of regional deformation zones and U-Pb dating of calcite slickenfibres provided absolute timing constraints of their activity as well as quantitative estimates of shortening rates.

The structural style of Miocene shortening is dominated by shallow rooted thrusting along a basal décollement. Thereby, the propagation of thrusting and the localization of the main deformation zones was largely controlled by the configuration of pre-existing basement faults (most importantly the Late Paleozoic CFT) and structures that inherited from them prior to thrusting. The latter caused some lateral changes in the structural style of faults observed in the sedimentary cover.

Concerning deformation timing, the main phase of thin-skinned foreland deformation *sensu stricto* (e.g., with contractional deformation solely occurring in the Mesozoic cover) is well constrained for the time period between 14 and 8 Ma. Thereby, the main thrust front formed relatively early. It was followed by further deformation in the hinterland but also continued foreland propagation. The latter continued until at least ~4 Ma and occurred contemporaneously with normal faulting in the eastern part of the study area. This is interpreted as strain partitioning during foreland tectonics. From a regional perspective, deep-seated contractional reactivation of basement structures (e.g., thick-skinned tectonics) appear to only have played a minor role during the latest phase of foreland deformation.

Cumulative rates of predominately thin-skinned deformation derived from balanced cross section range between ~0.9 and ~0.1 mm/year with rates decreasing toward the eastern tip of the arcuate fold-and-thrust belt.

Furthermore, it appears that the initial thin-skinned deformation occurred at significantly higher rates than the later deformation increments north of the main deformation front.

Our case study from a classical foreland setting showcases how U-Pb calcite dating can be applied to unravel deformation sequences and shortening estimates of foreland fold-and-thrust belts. Thereby, the interpretation of the latter data is not straight-forward and must be based on a sound understanding of meso-scale (fracture kinematics) and regional tectonics (large-scale deformation style). The promise held by this approach is to improve our understanding of fold-and-thrust belt evolution not only in space, but also time.

### Data Availability Statement

All new data presented in this article are available to the public at the data sharing infrastructure of EarthChem ([www.earthchem.org](http://www.earthchem.org)): <https://doi.org/10.60520/IEDA/113159>. Contents of the supporting information include structural data from outcrops and drill cores, sample photographs, cathodoluminescence microphotographs, Tera-Wasserburg concordia diagrams of samples, U-Pb data of samples and secondary reference materials, as well as LA-ICP-MS parameters and U-Pb metadata.

### Acknowledgments

U-Pb dating was carried out in the framework of a research project was funded by Nagra. Stefano Bernasconi (ETH Zürich) is acknowledged for his support in launching this project. Michael Schnellmann and Tim Vietor (both Nagra) are thanked for providing useful comments on the manuscript. HM would furthermore like to thank Christoph Eichkitz (Geo5 GmbH) and Beat Meier (formerly at Proseis AG) for previous collaborations on seismic interpretation. Two anonymous reviewers and associated editor Olivier Lacombe are thanked for their constructive comments that helped to improve the original manuscript.

### References

- Beaudoin, N., Lacombe, O., Roberts, N. M. W., & Koehn, D. (2018). U-Pb dating of calcite veins reveals complex stress evolution and thrust sequence in the Bighorn Basin, Wyoming, USA. *Geology*, *46*(11), 1015–1018. <https://doi.org/10.1130/G45379.1>
- Beck, C., Deville, E., Blanc, E., Philippe, Y., & Tardy, M. (1998). Horizontal shortening control of middle Miocene marine siliciclastic accumulation (upper Marine Molasse) in the Southern Termination of the Savoy Molasse Basin (northwestern Alps/southern Jura). *Geological Society Special Publications*, *134*, 263–278. <https://doi.org/10.1144/GSL.SP.1998.134.01.12>
- Becker, A. (2000). The Jura Mountains—An active foreland fold-and-thrust belt? *Tectonophysics*, *321*(4), 381–406. [https://doi.org/10.1016/S0040-1951\(00\)00089-5](https://doi.org/10.1016/S0040-1951(00)00089-5)
- Bilau, A., Bienvegnant, D., Rolland, Y., Schwartz, S., Godeau, N., Guihou, A., et al. (2023). The Tertiary structuration of the Western Subalpine foreland deciphered by calcite-filled faults and veins. *Earth-Science Reviews*, *236*, 104270. <https://doi.org/10.1016/j.earscirev.2022.104270>
- Bitterli-Brunner, P. (1987). Die Mandacher und Mettauer Aufschiebungen (Aargauer Tafeljura) aufgrund neuer Untersuchungen. *Bulletin der Vereinigung Schweizerischer Petroleum-Geologen und -Ingenieure*, *54*, 23–36.
- Burkhard, M. (1990). Aspects of the large-scale Miocene deformation in the most external part of the Swiss Alps (Subalpine Molasse to Jura fold belt). *Eclogae Geologicae Helveticae*, *83*, 559–583.
- Burkhard, M., & Sommaruga, A. (1998). Evolution of the western Swiss Molasse basin: Structural relations with the Alps and the Jura belt, in Cenozoic Foreland Basins of Western Europe. *Geological Society Special Publications*, *134*(1), 279–298. <https://doi.org/10.1144/GSL.SP.1998.134.01.13>
- Butler, R. W. H., Bond, C. E., Cooper, M. A., & Watkins, H. (2018). Interpreting structural geometry in fold-thrust belts: Why style matters. *Journal of Structural Geology*, *114*, 251–273. <https://doi.org/10.1016/j.jsg.2018.06.019>
- Butler, R. W. H., Tavarnelli, E., & Grasso, M. (2006). Structural inheritance in mountain belts: An Alpine-Apennine perspective. *Journal of Structural Geology*, *28*(11), 1893–1908. <https://doi.org/10.1016/j.jsg.2006.09.006>
- Buxtorf, A. (1907). Geologische Beschreibung des Weissenstein Tunnels und seiner Umgebung. In *Beitraege der Geologischen Karte der Schweiz*. Schweiz. Geol. Kommission.
- Calamita, F., Pace, P., Scisciani, V., Properzi, F., & Francioni, M. (2021). Dinaric up-thrusts in the Pliocene evolution of the Central Apennines thrust belt of Italy: The Montagna dei Fiori structure. *Geological Magazine*, *158*(11), 2063–2078. <https://doi.org/10.1017/S0016756821000613>
- Carola, E., Muñoz, J. A., & Roca, E. (2015). The transition from thick-skinned to thin-skinned tectonics in the Basque-Cantabrian Pyrenees: The Burgalesa Platform and surroundings. *International Journal of Earth Sciences*, *104*(8), 2215–2239. <https://doi.org/10.1007/s00531-015-1177-z>
- Cederbom, C. E., Sinclair, H. D., Schlunegger, F., & Rahn, M. K. (2004). Climate-induced rebound and exhumation of the European Alps. *Geology*, *32*(8), 709–712. <https://doi.org/10.1130/g20491.1>
- Chapple, W. M. (1978). Mechanics of thin-skinned fold-and-thrust belts. *Geological Society of America Bulletin*, *89*(8), 1189–1198. [https://doi.org/10.1130/0016-7606\(1978\)89<1189:motfb>2.0.co;2](https://doi.org/10.1130/0016-7606(1978)89<1189:motfb>2.0.co;2)
- Coward, M. P. (1983). Thrust tectonics, thin skinned or thick skinned, and the continuation of thrusts to deep in the crust. *Journal of Structural Geology*, *5*(2), 113–123. [https://doi.org/10.1016/0191-8141\(83\)90037-8](https://doi.org/10.1016/0191-8141(83)90037-8)
- Cristallini, E. O., & Ramos, V. A. (2000). Thick-skinned and thin-skinned thrusting in the La Ramada fold and thrust belt: Crustal evolution of the High Andes of San Juan Argentina (32° SL). *Tectonophysics*, *317*(3–4), 205–235. [https://doi.org/10.1016/s0040-1951\(99\)00276-0](https://doi.org/10.1016/s0040-1951(99)00276-0)
- Dahlstrom, C. D. (1969). Balanced cross sections. *Canadian Journal of Earth Sciences*, *6*(4), 743–757. <https://doi.org/10.1139/e69-069>
- Davis, D., Suppe, J., & Dahlen, F. A. (1983). Mechanics of fold-and-thrust belts and accretionary wedges. *Journal of Geophysical Research*, *88*(B2), 1153–1172. <https://doi.org/10.1029/jb088ib02p01153>
- Deville, E., Blanc, E., Tardy, M., Beck, C., Cousin, M., & Menard, G. (1994). Thrust propagation and syntectonic sedimentation in the Savoy Tertiary Molasse basin (Alpine foreland). In A. Mascle (Ed.), *Hydrocarbon and petroleum geology of France* (Vol. 4, pp. 269–280). Springer. [https://doi.org/10.1007/978-3-642-78849-9\\_19](https://doi.org/10.1007/978-3-642-78849-9_19)
- Diebold, P. (1988). Der Nordschweizer Permokarbon-Trog und die Steinkohlenfrage der Nordschweiz. *Vierteljahrsschrift der Naturforschenden Gesellschaft in Zürich*, *133*(1), 143–174.
- Diebold, P., Bitterli-Brunner, P., & Naef, H. (2005). Blatt 1069 Frick mit schweizerischem Anteil von Blatt 1049 Laufenburg. In *Geologischer Atlas der Schweiz (1:25 000)*. swisstopo.
- Diebold, P., Naef, H., & Ammann, M. (1991). *Zur Tektonik der zentralen Nordschweiz. Interpretation aufgrund regionaler Seismik, Oberflächengeologie und Tiefbohrungen* (Technical Report NTB 90-04). Nagra.

- Diebold, P., & Noack, T. (1997). Late Paleozoic troughs and Tertiary structures in the eastern Folded Jura. In O. A. Pfiffner, P. Lehner, P. Heitzmann, S. Müller & A. Steck (Eds.), *Results of NRP 20* (pp. 59–63). Birkhäuser.
- Diehl, T., Madritsch, H., Schnellmann, S., Spillmann, T., Brockmann, E., & Wiemer, S. (2022). Seismotectonic evidence for present-day transtensional reactivation of the slow deforming Hegau-Bodensee Graben in the northern foreland of the Central Alps. *Tectonophysics*, 846, 229659. <https://doi.org/10.1016/j.tecto.2022.229659>
- Echtler, H. P., & Chauvet, A. (1992). Carboniferous convergence and subsequent crustal extension in the southern Schwarzwald (SW Germany). *Geodynamica Acta*, 5(1–2), 37–49. <https://doi.org/10.1080/09853111.1992.11105218>
- Egli, D., Mosar, J., Ibele, T., & Madritsch, H. (2017). The role of precursory structures on Tertiary deformation in the Black Forest-Hegau region. *International Journal of Earth Sciences*, 106(7), 2297–2318. <https://doi.org/10.1007/s00531-016-1427-8>
- Eisbacher, G. H., Lüschen, E., & Wickert, F. (1989). Crustal-scale thrusting and extension on the Hercynian Schwarzwald and Vosges, Central Europe. *Tectonics*, 8(1–21), 1–21. <https://doi.org/10.1029/TC008i001p00001>
- Ferrill, D. A., Smart, K. J., Cawood, A. J., & Morris, A. P. (2021). The fold-thrust belt stress cycle: Superposition of normal, strike-slip, and thrust faulting deformation regimes. *Journal of Structural Geology*, 148, 104362. <https://doi.org/10.1016/j.jsg.2021.104362>
- Gegg, L., Buechi, M., Ebert, A., Deplazes, G., Madritsch, H., & Anselmetti, F. S. (2020). Brecciation of glacially overridden palaeokarst (Lower Aare Valley, northern Switzerland): Result of subglacial water-pressure peaks? *Boreas*, 49(4), 813–827. <https://doi.org/10.1111/bor.12457>
- Geyer, M., Nisch, E., & Simon, T. (2011). *Geologie von Baden-Württemberg*. Schweizerbart.
- Giamboni, M., Ustaszewski, K., Schmid, S. M., Schumacher, M. E., & Wetzel, A. (2004). Plio-Pleistocene transpressional reactivation of Paleozoic and Paleogene structures in the Rhine-Bresse Transform Zone (northern Switzerland and eastern France). *International Journal of Earth Sciences*, 93(2), 207–223. <https://doi.org/10.1007/s00531-003-0375-2>
- Gorin, G., Signer, C., & Amberger, G. (1993). Structural configuration of the western Swiss Molasse Basin as defined by reflection seismic data. *Eclogae Geologicae Helveticae*, 86, 693–716.
- Graf, H. R., Bitterli-Dreher, Burger, H., Bitterli, T., Diebold, P., & Naef, H. (2006). Blatt 1070 Baden. In *Geologischer Atlas der Schweiz (1:25 000)*. swisstopo.
- Guillong, M., Wotzlaw, J., Looser, N., & Laurent, O. (2020). Evaluating the reliability of U–Pb laser ablation inductively coupled plasma mass spectrometry (LA-ICP-MS) carbonate geochronology: Matrix issues and a potential calcite validation reference material. *Geochronology*, 2(1), 155–167. <https://doi.org/10.5194/gchron-2-155-2020>
- Hamilton, W. B. (1988). Laramide crustal shortening. In C. J. Schmidt & W. J. Perry (Eds.), *Interaction of the rocky mountain foreland and the cordilleran thrust belt, Geological Society of America Memoir* (Vol. 171, pp. 27–39).
- Hammer, P., Ibele, T., Naef, H., & Madritsch, H. (2019). *Geomorphologische Analyse der Basis der Höheren Deckenschotter im Gebiet Nördlich Lägern* (Project Report NAB 15-057). Nagra.
- Herwegh, M., Berger, A., Glotzbach, C., Wangenheim, C., Mock, S., Wehrens, P., et al. (2019). Late stages of continent-continent collision: Timing, kinematic evolution, and exhumation of the northern rim (Aar Massif) of the Alps. *Earth-Science Reviews*, 200, 102959. <https://doi.org/10.1016/j.earscirev.2019.102959>
- Hofmann, F., Schlatter, R., & Weh, M. (2000). Blatt 1011 Beggingen (Südhälfte) mit SW-Anteil von Blatt 1012 Singen. In *Geologischer Atlas der Schweiz (1:25 000)*. swisstopo.
- Hölker, A., & Birkhäuser, P. (2018). *3D Seismik Datenbearbeitung 2016-17* (Project Report NAB 17-36). Nagra.
- Homberg, C., Lacombe, O., Angelier, J., & Bergerat, F. (1999). New constraints for indentation mechanisms in arcuate belts from the Jura Mountains, France. *Geology*, 27(9), 827–830. [https://doi.org/10.1130/0091-7613\(1999\)027<0827:ncfimi>2.3.co;2](https://doi.org/10.1130/0091-7613(1999)027<0827:ncfimi>2.3.co;2)
- Illies, J. H. (1972). The Rhinegraben Rift System—Plate tectonics and transform faulting. *Geophysical Surveys*, 1, 27–60. <https://doi.org/10.1007/BF01449550>
- Jordan, P. (1992). Evidence for large-scale decoupling in the Triassic evaporites of northern Switzerland—An overview. *Eclogae Geologicae Helveticae*, 85, 677–693.
- Jordan, P., Malz, A., Heuberger, S., Pietsch, J., Kley, J., & Madritsch, H. (2015). *Regionale geologische Profilschnitte durch die Nordschweiz und 2D-Bilanzierung der Fernschubdeformation im östlichen Faltenjura* (Project Report NAB 14-105). Nagra.
- Kastrup, U., Zoback, M. L., Deichmann, N., Evans, K. F., Giardini, D., & Michael, A. J. (2004). Stress field variations in the Swiss Alps and the northern Alpine foreland derived from inversion of fault plane solutions. *Journal of Geophysical Research*, 109(B1), B01402. <https://doi.org/10.1029/2003JB002550>
- Kempf, O., & Pfiffner, O. A. (2004). Early Tertiary evolution of the North Alpine Foreland Basin of the Swiss Alps and adjoining areas. *Basin Research*, 16(4), 549–567. <https://doi.org/10.1111/j.1365-2117.2004.00246.x>
- Kissling, E., & Schlunegger, F. (2018). Rollback orogeny model for the evolution of the Swiss Alps. *Tectonics*, 37(4), 1097–1115. <https://doi.org/10.1002/2017tc004762>
- Kuhlemann, J., & Rahn, M. (2013). Plio-Pleistocene landscape evolution in Northern Switzerland. *Swiss Journal of Geosciences*, 106(3), 451–467. <https://doi.org/10.1007/s00015-013-0152-6>
- Lacombe, O., & Beaudoin, N. E. (2023). Timing, sequence, duration and rate of deformation in fold-and-thrust belts: A review of traditional approaches and recent advances from absolute dating (K–Ar illite/U–Pb calcite) of brittle structures. *Comptes Rendus Geoscience*, 356(S2), 1–28. <https://doi.org/10.5802/crgeos.218>
- Lacombe, O., Beaudoin, N. E., Hoareau, G., Labeur, A., Pecheyran, C., & Callot, J.-P. (2021). Dating folding beyond folding, from layer-parallel shortening to fold tightening, using mesostructures: Lessons from the Apennines, Pyrenees, and Rocky Mountains. *Solid Earth*, 12(10), 2145–2157. <https://doi.org/10.5194/se-12-2145-2021>
- Lacombe, O., & Bellahsen, N. (2016). Thick-skinned tectonics and basement-involved fold-thrust belts: Insights from selected Cenozoic orogens. *Geological Magazine*, 153(5–6), 763–810. <https://doi.org/10.1017/s0016756816000078>
- Lacombe, O., & Mouthereau, F. (2002). Basement-involved shortening and deep detachment tectonics in forelands of orogens: Insights from recent collision belts (Taiwan, western Alps, Pyrenees). *Tectonics*, 21(4), 12–21. <https://doi.org/10.1029/2001tc901018>
- Lacombe, O., Mouthereau, F., Angelier, J., Chu, H.-T., & Lee, J.-C. (2003). Frontal curvature and oblique ramp development at an obliquely collided irregular margin: Geometry and kinematics of the NW Taiwan fold-thrust belt. *Tectonics*, 22(3), 1025. <https://doi.org/10.1029/2002TC001436>
- Lanza, F., Diehl, T., Deichmann, N., Kraft, T., Nussbaum, C., Schefer, S., & Wiemer, S. (2022). The Saint-Ursanne earthquakes of 2000 revisited: Evidence for active shallow thrust-faulting in the Jura fold-and-thrust belt. *Swiss Journal of Geosciences*, 115(2), 2. <https://doi.org/10.1186/s00015-021-00400-x>
- Laubscher, H. (1961). Die Fernschubhypothese der Jurafaltung. *Eclogae Geologicae Helveticae*, 54, 222–282.

- Laubscher, H. (1972). Some overall aspects of Jura dynamics. *American Journal of Science*, 272(4), 293–304. <https://doi.org/10.2475/ajs.272.4.293>
- Laubscher, H. (1986). The eastern Jura: Relations between thin-skinned and basement tectonics, local and regional. *Geologische Rundschau*, 75(3), 535–553. <https://doi.org/10.1007/BF01820630>
- Looser, N., Madritsch, H., Guillong, M., Laurent, O., Wohlwend, S., & Bernasconi, S. (2021). Absolute age and temperature constraints on deformation along the basal décollement of the Jura fold-and-thrust belt from carbonate U-Pb dating and clumped isotopes. *Tectonics*, 40(3), e2020TC006439. <https://doi.org/10.1029/2020TC006439>
- Madritsch, H. (2015). Outcrop-scale fracture systems in the Alpine foreland of central Northern Switzerland: Kinematics and tectonic context. *Swiss Journal of Geosciences*, 108(2–3), 155–181. <https://doi.org/10.1007/s00015-015-0203-2>
- Madritsch, H., Naef, H., Meier, B., Franzke, J. A., & Schreurs, G. (2018). Architecture and kinematics of the Constance-Frick Trough (Northern Switzerland): Implications for the formation of post-Variscan basins in the foreland of the Alps and scenarios of their Neogene reactivation. *Tectonics*, 37(7), 2197–2220. <https://doi.org/10.1029/2017TC004945>
- Madritsch, H., Preusser, F., Fabbri, O., Bichet, V., Schlunegger, F., & Schmid, S. (2010). Late Quaternary folding in the Jura Mountains: Evidence from syn-erosional deformation of fluvial meanders. *Terra Nova*, 22(2), 147–154. <https://doi.org/10.1111/j.1365-3121.2010.00928.x>
- Madritsch, H., Schmid, S. M., & Fabbri, O. (2008). Interactions between thin- and thick-skinned tectonics at the northwestern front of the Jura fold-and-thrust belt (Eastern France). *Tectonics*, 27(5), TC5005. <https://doi.org/10.1029/2008TC002282>
- Malz, A., Madritsch, H., Jordan, P., Meier, B., & Kley, J. (2019). Along-strike variations in thin-skinned thrusting style controlled by pre-existing basement structure in the easternmost Jura Mountains (northern Switzerland). *Geological Society Special Publications*, 490, 199–220.
- Malz, A., Madritsch, H., & Kley, J. (2015). Improving 2D-seismic interpretation in challenging settings by integration of restoration techniques: A case study from the Jura fold-and-thrust belt (Switzerland). *Interpretation*, 3(4), SAA37–SAA58. <https://doi.org/10.1190/INT-2015-0012.1>
- Malz, A., Madritsch, H., Meier, B., & Kley, J. (2016). An unusual triangle zone in the external northern Alpine foreland (Switzerland): Structural inheritance, kinematics and implications for the development of the adjacent Jura fold-and-thrust belt. *Tectonophysics*, 670, 127–143. <https://doi.org/10.1016/j.tecto.2015.12.025>
- Marchant, R., Ringgenberg, Y., Stampfli, G., Birkhäuser, P., Roth, P., & Meier, B. (2005). Paleotectonic evolution of the Zürcher Weinland (northern Switzerland) based on 2D and 3D seismic data. *Eclogae Geologicae Helveticae*, 98(3), 345–362. <https://doi.org/10.1007/s00015-005-1171-8>
- Mazurek, M., Hurford, A. J., & Leu, W. (2006). Unravelling the multi-stage burial history of the Swiss Molasse Basin: Integration of apatite fission track, vitrinite reflectance and biomarker isomerization analysis. *Basin Research*, 18(1), 27–50. <https://doi.org/10.1111/j.1365-2117.2006.00286>
- McCann, T., Pascal, C., Timmerman, M. J., Krzywiec, P., López-Gómez, J., Wetzel, A., et al. (2006). Post-Variscan (end Carboniferous – Early Permian) basin evolution in Western and Central Europe. In D. G. Gee & R. A. Stephenson (Eds.), *European lithosphere dynamics* (pp. 355–388). Geological Society.
- Meier, B., Kuhn, P., Roth, P., & Madritsch, H. (2014). *Tiefenkonvertierung der regionalen Strukturinterpretation der Nagra 2D-Seismik 2011/12* (Project Report NAB 14-34). Nagra.
- Meigs, A., Krugh, W. C., Schiffmann, C., Vergés, J., & Ramos, V. A. (2006). Refolding of thin-skinned thrust sheets by active basement-involved thrust faults in the Eastern Precordillera of western Argentina. *Revista de la Asociación Geológica Argentina*, 61, 589–603.
- Mitra, S., & Namson, J. (1989). Equal-area balancing. *American Journal of Science*, 289(5), 563–599. <https://doi.org/10.2475/ajs.289.5.563>
- Mock, S., & Herwegh, M. (2017). Tectonics of the Swiss Molasse Basin: Post Miocene transition to incipient thick-skinned tectonics? *Tectonics*, 36(9), 1699–1723. <https://doi.org/10.1002/2017TC004584>
- Mock, S., von Hagke, C., Schlunegger, F., Dunkl, I., & Herwegh, M. (2020). Long wavelength Late-Miocene thrusting in the North Alpine foreland. Implication for late orogenic processes. *Solid Earth*, 11(5), 1823–1847. <https://doi.org/10.5194/se-11-1823-2020>
- Molinario, M., Leturmy, J.-C., Guezou, D., D., De Lamotte, F., & Eshraghi, S. A. (2005). The structure and kinematics of the southeastern Zagros foldthrust belt Iran: From thin-skinned to thick-skinned tectonics. *Tectonics*, 24(3), TC3007. <https://doi.org/10.1029/2004TC001633>
- Mosar, J. (1999). Present-day and future tectonic underplating in the western Swiss Alps: Reconciliation of basement/wrench-faulting and décollement folding in the Jura and Molasse basin in the Alpine foreland. *Earth and Planetary Science Letters*, 73(3), 143–155. [https://doi.org/10.1016/S0012-821X\(99\)00238-1](https://doi.org/10.1016/S0012-821X(99)00238-1)
- Müller, W. H., Naef, H., & Graf, H. R. (2002). *Geologische Entwicklung der Nordschweiz, Neotektonik und Langzeitszenarien Zürcher Weinland [mit Korrigendum]* (Technical Report NTB 99-08). Nagra.
- Naef, H., Birkhäuser, P., & Roth, P. (1995). *Interpretation der Reflexionsseismik im Gebiet nördlich Lägeren – Zürcher Weinland* (Technical Report NTB 94–14). Nagra.
- Nagra. (2014). *SGT Etappe 2: Vorschlag weiter zu untersuchender geologischer Standortgebiete mit zugehörigen Standortarealen für die Oberflächenanlage – Geologische Grundlagen* (Technical Report NTB 14–02/II). Nagra.
- Nagra. (2019a). *Preliminary horizon and structure mapping of the Nagra 3D seismic JO-15 (Jura Ost) in time domain* (Project Report NAB 18-34). Nagra.
- Nagra. (2019b). *Preliminary horizon and structure mapping of the Nagra 3D seismic NL 16 (Nördlich Lägern) in time domain* (Project Report NAB 18-35). Nagra.
- Nagra. (2019c). *Preliminary horizon and structure mapping of the Nagra 3D seismic ZNO 96/17 (Zürich Nordost) in time domain* (Project Report NAB 18-36). Nagra.
- Nagra. (2021a). *TBO Bülach-1-1: Data Report Dossier I-XI* (Project Report NAB 20-08). Nagra.
- Nagra. (2021b). *TBO Marthalen-1-1: Data Report Dossier I-XI* (Project Report NAB 21-20). Nagra.
- Nagra. (2021c). *TBO Trüllikon-1-1: Data Report Dossier I-XI* (Project Report NAB 20-09). Nagra.
- Nagra. (2022a). *TBO Bözberg-1-1: Data Report Dossier I-XI* (Project Report NAB 21-21). Nagra.
- Nagra. (2022b). *TBO Bözberg-2-1: Data Report Dossier I-XI* (Project Report NAB 21-22). Nagra.
- Nagra. (2022c). *TBO Stadel-2-1: Data Report Dossier I-XI* (Project Report NAB 22-02). Nagra.
- Nagra. (2022d). *TBO Stadel-3-1: Data Report Dossier I-XI* (Project Report NAB 22-01). Nagra.
- Nemcok, M., Schamel, S., & Gayer, R. (2009). *Thrustbelts: Structural architecture, thermal regimes and petroleum systems* (pp. 1–541). University Press. <https://doi.org/10.1017/CBO9780511584244>
- Nivière, B., & Winter, T. (2000). Pleistocene northwards fold propagation of the Jura within the southern Upper Rhine Graben: Seismotectonic implications. *Global and Planetary Change*, 27(1–4), 263–288. [https://doi.org/10.1016/S0921-8181\(01\)00070-4](https://doi.org/10.1016/S0921-8181(01)00070-4)
- Nuriel, P., Weinberger, R., Kylander-Clark, A. R. C., Hacker, B. R., & Craddock, J. P. (2017). The onset of the dead sea transform based on calcite age-strain analyses. *Geology*, 45(7), 587–590. <https://doi.org/10.1130/G38903.1>

- Nuriel, P., Wotzlaw, J.-F., Ovtcharova, M., Vaks, A., Stremtan, C., Šala, M., et al. (2020). The use of ASH-15 flowstone as a matrix-matched reference material for laser-ablation U-Pb geochronology of calcite. *Geochronology*, 3, 35–47. <https://doi.org/10.5194/gchron-2020-22>
- Nussbaum, C., Kloppenburg, A., Caër, T., & Bossart, P. (2017). Tectonic evolution around the Mont Terri rock laboratory, northwestern Swiss Jura: Constraints from kinematic forward modelling. *Swiss Journal of Geosciences*, 110(1), 39–66. <https://doi.org/10.1007/s00015-016-0248-x>
- Ortner, H., von Hagke, C., Sommaruga, A., Mock, S., Mosar, J., Hinsch, R., & Beidinger, A. (2023). The northern deformation front of the European Alps. In N. Bellahsen & C. Rosenberg (Eds.), *Geodynamics of the Alps 3*. ISTE-Wiley.
- Pace, P., Domenica, A. D., & Calamita, F. (2014). Summit low-angle faults in the Central Apennines of Italy: Younger-on-older thrusts or rotated normal faults? Constraints for defining the tectonic style of thrust belts. *Tectonics*, 33(5), 756–785. <https://doi.org/10.1002/2013TC003385>
- Parrish, R. R., Parrish, C. M., & Lasalle, S. (2018). Vein calcite dating reveals Pyrenean orogen as cause of Paleogene deformation in southern England. *Journal of the Geological Society*, 175(3), 425–442. <https://doi.org/10.1144/jgs2017-107>
- Pfiffner, O. A. (1986). Evolution of the North Alpine foreland basin in the Central Alps. In P. A. Allen & P. Homewood (Eds.), *Foreland Basins, International Association of Sedimentologists, special publications* (Vol. 8, pp. 219–228). Blackwell Publishing Ltd.
- Pfiffner, O. A. (2006). Thick-skinned and thin-skinned styles of continental contraction. *Geological Society of America Special Papers*, 414, 153–177.
- Pfiffner, O. A. (2017). Thick-skinned and thin-skinned tectonics: A global perspective. *Geosciences*, 7(3), 71. <https://doi.org/10.3390/geosciences7030071>
- Pfiffner, O. A., Erard, P. F., & Stäubli, M. (1997). Two cross sections through the Swiss Molasse Basin (lines E4-E6, W1, W7-W10). In O. A. Pfiffner, P. Lehner, P. Heitzmann, S. Müller & A. Steck (Eds.), *Deep structure of the Swiss Alps. Results of NRP 20* (pp. 64–72). Birkhäuser.
- Poblet, J., & Lisle, R. J. (2011). Kinematic evolution and structural styles of fold-and-thrust belts. *Geological Society Special Publications, Geological Society of London*, 349, 1–24. <https://doi.org/10.1144/SP349.1>
- Radaideh, O. M. A., & Mosar, J. (2021). Cenozoic tectonic deformation along the Pontarlier Strike-Slip Fault Zone (Swiss and French Jura Fold-and-Thrust Belt): Insights from paleostress and geomorphic analyses. *Tectonics*, 40(5), e2021TC006758. <https://doi.org/10.1029/2021TC006758>
- Rahn, M., & Selbekk, R. (2007). Absolute dating of the youngest sediments of the Swiss Molasse basin by apatite fission track analysis. *Swiss Journal of Geosciences*, 100(3), 371–381. <https://doi.org/10.1007/s00015-007-1234-0>
- Ring, U., & Gerdes, A. (2016). Kinematics of the Alpenrhein-Bodensee graben system in the Central Alps: Oligocene/Miocene transtension due to formation of the Western Alps arc. *Tectonics*, 35(6), 1367–1391. <https://doi.org/10.1002/2015tc004085>
- Rittner, M. (2013). U-Pb dating of brittle deformation (Unpublished Doctoral Thesis) (p. 270). Royal Holloway University of London. Retrieved from [https://pure.royalholloway.ac.uk/portal/en/publications/upb-dating-of-brittle-deformation\(aff86bf1-7949-4184-88c1-886cc509dfc2\).html](https://pure.royalholloway.ac.uk/portal/en/publications/upb-dating-of-brittle-deformation(aff86bf1-7949-4184-88c1-886cc509dfc2).html)
- Roberts, N. M. W., Rasbury, E. T., Parrish, R. R., Smith, C. J., Horstwood, M. S. A., & Condon, D. J. (2017). A calcite reference material for LA-ICP-MS U-Pb geochronology. *Geochemistry, Geophysics, Geosystems*, 18(7), 2807–2814. <https://doi.org/10.1002/2016GC006784>
- Roche, V., Childs, C., Madritsch, H., & Camanni, G. (2020). Layering and structural inheritance controls on fault zone structure in three dimensions: A case study from the northern Molasse Basin, Switzerland. *Journal of the Geological Society*, 177(3), 493–508. <https://doi.org/10.1144/jgs2019-052>
- Rotstein, Y., & Schaming, M. (2004). Seismic reflection evidence for thick-skinned tectonics in the northern Jura. *Terra Nova*, 16(5), 250–256. <https://doi.org/10.1111/j.1365-3121.2004.00560.x>
- Schaltegger, U. (2000). U-Pb geochronology of the southern Black Forest Batholith (Central Variscian Belt): Timing of exhumation and granite emplacement. *International Journal of Earth Sciences*, 88(4), 814–828. <https://doi.org/10.1007/s005310050308>
- Schlunegger, F., & Mosar, J. (2011). The last erosional stage of the Molasse Basin and the Alps. *International Journal of Earth Sciences*, 100(5), 1147–1162. <https://doi.org/10.1007/s00531-010-0607-1>
- Schmid, S. M., Fuegenschuh, B., Kissling, E., & Schuster, R. (2004). Tectonic map and overall architecture of the Alpine orogen. *Eclogae Geologicae Helveticae*, 97(1), 93–117. <https://doi.org/10.1007/s00015-004-1113-x>
- Schöpfer, K., Decker, K., Nazari, F., & Madritsch, H. (2023). 3D seismic evidence for thick-skinned tectonics in a “classic” thin-skinned tectonics region (external Alpine foreland, Switzerland). *Terra Nova*, 00, 1–13. <https://doi.org/10.1111/ter.12701>
- Schori, M. (2022). The development of the Jura fold and thrust belt: Pre-existing basement structures and the formation of ramps (Doctoral Dissertation), Geofocus (Vol. 50, p. 200). University of Fribourg. Retrieved from <https://doi.org/10.51363/unifr.sth.2022.001>
- Schori, M., Mosar, J., & Schreurs, G. (2015). Multiple detachments during thin-skinned deformation of the Swiss central Jura: A kinematic model across the Chasseral. *Swiss Journal of Geosciences*, 108(2–3), 327–343. <https://doi.org/10.1007/s00015-015-0196-x>
- Schori, M., Zwaan, F., Schreurs, G., & Mosar, J. (2021). Pre-existing basement faults controlling deformation in the Jura Mountains fold-and-thrust belt: Insights from analogue models. *Tectonophysics*, 814, 228980. <https://doi.org/10.1016/j.tecto.2021.228980>
- Schreiner, A. (1992). Hegau und westlicher Bodensee. In *Geologische Karte von Baden-Württemberg (1:50 000)* (p. 290). LRGB.
- Schumacher, M. E. (2002). Upper Rhine Graben: Role of preexisting structures during rift evolution. *Tectonics*, 21(1), 6–16. <https://doi.org/10.1029/2001TC900022>
- Sinclair, H. D., & Allen, P. A. (1992). Vertical versus horizontal motions in the Alpine orogenic wedge: Stratigraphic response in the foreland basin. *Basin Research*, 4(3–4), 215–232. <https://doi.org/10.1111/j.1365-2117.1992.tb00046.x>
- Smeraglia, L., Looser, N., Fabbri, O., Choulet, F., Guillong, M., & Bernasconi, S. M. (2021). U-Pb dating of middle Eocene Pleistocene multiple tectonic pulses in the Alpine foreland. *Solid Earth*, 12(11), 2539–2551. <https://doi.org/10.5194/se-12-2539-2021>
- Sommaruga, A. (1999). Décollement tectonics in the Jura foreland fold-and-thrust belt. *Marine and Petroleum Geology*, 16(2), 111–134. [https://doi.org/10.1016/s0264-8172\(98\)00068-3](https://doi.org/10.1016/s0264-8172(98)00068-3)
- Sommaruga, A., Eichenberger, U., & Mariller, F. (2012). *Seismic Atlas of the Swiss Molasse Basin*. swisstopo.
- Sommaruga, A., Mosar, J., Schori, M., & Gruber, M. (2017). The role of the Triassic evaporites underneath the North Alpine foreland. In J. I. Soto, J. Flinch, & G. Tari (Eds.), *Permo-Triassic salt provinces of Europe, North Africa and the Atlantic Margins* (pp. 447–466). Elsevier.
- Tavani, S., Camanni, G., Nappo, M., Snidero, M., Ascione, A., Valente, E., et al. (2021). The Mountain Front Flexure in the Lurestan region of the Zagros belt: Crustal architecture and role of structural inheritances. *Journal of Structural Geology*, 135, 104022. <https://doi.org/10.1016/j.jsg.2020.104022>
- Tavani, S., Parente, M., Puzone, F., Corradetti, A., Gharabegli, G., Mehdi Valinejad, M., et al. (2018). The seismogenic fault system of the 2017  $M_w$  7.3 Iran–Iraq earthquake: Constraints from surface and subsurface data, cross-section balancing, and restoration. *Solid Earth*, 9(3), 821–831. <https://doi.org/10.5194/se-9-821-2018>
- Tavani, S., Smeraglia, L., Fabbri, S., Aldega, L., Sabbatino, M., Cardello, G. L., et al. (2023). Timing, thrusting mode, and negative inversion along the Circeo thrust, Apennines, Italy: How the accretion-to-extension transition operated during slab rollback. *Tectonics*, 42(6), e2022TC007679. <https://doi.org/10.1029/2022TC007679>

- Tavani, S., Storti, F., Lacombe, O., Corradetti, A., Muñoz, J. A., & Mazzoli, S. (2015). A review of deformation pattern templates in foreland basin systems and fold-and-thrust belts: Implications for the state of stress in the frontal regions of thrust wedges. *Earth-Science Reviews*, *141*, 82–104. <https://doi.org/10.1016/j.earscirev.2014.11.013>
- Ustaszewski, K., & Schmid, S. M. (2006). Control of preexisting faults on geometry and kinematics in the northernmost part of the Jura fold-and-thrust belt. *Tectonics*, *25*(5), TC5003. <https://doi.org/10.1029/2005TC001915>
- Ustaszewski, K., & Schmid, S. M. (2007). Latest Pliocene to recent thick-skinned tectonics at the Upper Rhine Graben – Jura Mountains junction. *Swiss Journal of Geosciences*, *100*(2), 293–312. <https://doi.org/10.1007/s00015-007-1226-0>
- Vermeesch, P. (2018). IsoplotR: A free and open toolbox for geochronology. *Geoscience Frontiers*, *9*(5), 1479–1493. <https://doi.org/10.1016/j.gsf.2018.04.001>
- von Hagke, C., Cederbom, C. E., Oncken, O., Steckli, D. F., Rahn, M. K., & Schlunegger, F. (2012). Linking the northern Alps with their foreland: The latest exhumation history resolved by low-temperature thermochronology. *Tectonics*, *31*(5), TC5010. <https://doi.org/10.1029/2011TC003078>
- Watkins, H., Butler, R. W. H., & Bond, C. E. (2017). Using laterally compatible cross sections to infer fault growth and linkage models in foreland thrust belts. *Journal of Structural Geology*, *96*, 102–117. <https://doi.org/10.1016/j.jsg.2017.01.010>
- Werner, W., & Franzke, H. J. (2001). Postvariszische bis neogene Bruchtektonik und Mineralisation im südlichen Zentralschwarzwald. *Zeitschrift der Deutschen Geologischen Gesellschaft*, *152*(2–4), 405–437. <https://doi.org/10.1127/zdgg/152/2001/405>
- Wetzel, A., Allenbach, R., & Allia, V. (2003). Reactivated basement structures affecting the sedimentary facies in a tectonically “quiescent” epicontinental basin: An example from NW Switzerland. *Sedimentary Geology*, *157*(1), 153–172. [https://doi.org/10.1016/s0037-0738\(02\)00230-0](https://doi.org/10.1016/s0037-0738(02)00230-0)
- Wildi, W. (1975). Die Mettaufer Überschiebung im Aargauischen Tafeljura (Nordschweiz). *Eclogae Geologicae Helveticae*, *68*, 483–489.
- Ziegler, P. A. (1992). European Cenozoic Rift System. *Tectonophysics*, *208*(1–3), 91–111. [https://doi.org/10.1016/0040-1951\(92\)90338-7](https://doi.org/10.1016/0040-1951(92)90338-7)
- Ziegler, P. A., & Dèzes, P. (2006). Crustal evolution of Western and Central Europe. *Geological Society, London Memoirs*, *32*(1), 43–56. <https://doi.org/10.1144/gsl.mem.2006.032.01.03>